



Circadian ribosome profiling reveals a role for the *Period2* upstream open reading frame in sleep

Arthur Millius^{a,b,c} , Rikuhiko G. Yamada^a, Hiroshi Fujishima^a, Kazuhiko Maeda^b , Daron M. Standley^c , Kenta Sumiyama^d , Dimitri Perrin^{e,f} , and Hiroki R. Ueda^{a,g,1}

Edited by Joseph Takahashi, The University of Texas Southwestern Medical Center, Dallas, TX; received August 30, 2022; accepted August 29, 2023

Many mammalian proteins have circadian cycles of production and degradation, and many of these rhythms are altered posttranscriptionally. We used ribosome profiling to examine posttranscriptional control of circadian rhythms by quantifying RNA translation in the liver over a 24-h period from circadian-entrained mice transferred to constant darkness conditions and by comparing ribosome binding levels to protein levels for 16 circadian proteins. We observed large differences in ribosome binding levels compared to protein levels, and we observed delays between peak ribosome binding and peak protein abundance. We found extensive binding of ribosomes to upstream open reading frames (uORFs) in circadian mRNAs, including the core clock gene *Period2* (*Per2*). An increase in the number of uORFs in the 5'UTR was associated with a decrease in ribosome binding in the main coding sequence and a reduction in expression of synthetic reporter constructs. Mutation of the *Per2* uORF increased luciferase and fluorescence reporter expression in 3T3 cells and increased luciferase expression in PER2:LUC MEF cells. Mutation of the *Per2* uORF in mice increased *Per2* mRNA expression, enhanced ribosome binding on *Per2*, and reduced total sleep time compared to that in wild-type mice. These results suggest that uORFs affect mRNA posttranscriptionally, which can impact physiological rhythms and sleep.

circadian rhythms | ribosome profiling | uORF | mass spectrometry | RNA

Life is remarkably adapted to the 24-hour rotational movement of the earth. In mammals, the molecular time-keeping mechanism for circadian rhythms relies primarily on a hierarchical network of transcription activators and repressors in cells and tissues (1). In the past, circadian clocks have been measured using systems approaches to quantify genome-wide changes in RNA levels (2), which has resulted in an understanding of the transcriptional regulatory network; however, less is known about how translation and posttranscriptional regulation influence biological rhythms.

About 10% of genes in the liver have circadian oscillations in the steady-state levels of mRNA (3), but rhythmic transcription accounts for only some of these rhythms (4). For example, the timing of when a circadian mRNA is expressed does not necessarily correspond to that of mRNA translation or peak protein abundance (5). Some proteins have 24-h rhythms in abundance in the absence of rhythmic RNA expression (6, 7), which may suggest a role for rhythmic translation in regulating the clock (8).

In mouse liver, detection of low-abundant components of the core circadian circuit using systems proteomics is difficult (8, 9), unless special care is taken to examine a particular protein on a case-by-case basis (10) or by using advanced mass spectrometry techniques (11, 12). Researchers have used next-generation sequencing of ribosome-bound mRNA protected from RNase degradation to understand how translation regulation affects protein output (13, 14). Previous studies using ribosome profiling to measure daily rhythms focused on a cell culture model (15) or mouse tissues in light–dark conditions (16–18) to examine rhythms in diurnal gene expression, which may be influenced by noncircadian time-keeping systems. These studies also examined the timing between RNA abundance and ribosome binding, but it remains unclear how circadian translation relates to peak protein abundance in terms of protein turnover and timing. For example, the peak abundance of PER and CRY proteins is delayed relative to the expression of their mRNA in the liver (19) and suprachiasmatic nuclei (SCN) (20). This difference in timing may result from a delay in RNA processing before translation, a delay during translation, a delay in protein transport from one cellular location to another, or a delay in protein turnover (21, 22).

Previously, we developed a mass spectrometry method called MS-based Quantification By isotope-labeled Cell-free products (MS-QBiC) to determine the absolute protein levels of 16 selected circadian proteins in mice liver over a 24-h period (10). This method takes advantage of the PURE system (23) for reconstituting cell-free protein expression of

Significance

Period (*Per*) is an iconic gene in the field of circadian rhythms since its discovery in 1971 by Seymour Benzer and Ronald Konopka in fruit flies. The inhibitory feedback loop of PER protein drives circadian rhythms. We show that *Per2* is regulated by an upstream open reading frame (uORF) in the 5' untranslated region of the *Per2* mRNA. Mutation of the *Per2* uORF altered the amplitude of luciferase reporter expression in well-characterized cell culture models. *Per2* uORF mutant mice had significantly elevated *Per2* mRNA levels and exhibited sleep loss, particularly during light-to-dark and dark-to-light transitions, which suggests a role for uORFs in modulating molecular and physiological circadian rhythms.

Author contributions: A.M., R.G.Y., K.S., D.P., and H.R.U. designed research; A.M., R.G.Y., H.F., and K.S. performed research; K.M. and D.M.S. contributed new reagents/analytic tools; A.M. and D.P. analyzed data; and A.M. wrote the paper.

The authors declare no competing interest.

This article is a PNAS Direct Submission.

Copyright © 2023 the Author(s). Published by PNAS. This open access article is distributed under Creative Commons Attribution License 4.0 (CC BY).

¹To whom correspondence may be addressed. Email: uedah-ty@umin.ac.jp.

This article contains supporting information online at <https://www.pnas.org/lookup/suppl/doi:10.1073/pnas.2214636120/-/DCSupplemental>.

Published September 28, 2023.

optimal peptide standards for detection and quantification by selected reaction monitoring-based targeted proteomics analysis. We found delays between the peak levels of RNA expression, as measured by qPCR, and the abundance of the corresponding protein, suggesting either a delay in posttranscriptional RNA processing or in protein turnover. Here, we investigated the same liver samples by ribosome profiling in order to understand the timing of ribosome binding compared to peak protein and RNA levels. We found that upstream open reading frames (uORFs) modulated translation globally, repressed reporter expression in a combinatorial manner, and suppressed expression of *Per2*. Mutation of the *Per2* uORF in mice reduced total sleep duration, particularly during the early morning and early evening, without disrupting the circadian period, which suggests that uORF-mediated repression may impact physiological behaviors.

Results

Ribosome Profiling of the Liver from Mice in Constant Darkness Conditions. An experimental workflow was designed to analyze ribosome-protected mRNA fragments from liver samples previously examined by MS-QBiC (10) (*SI Appendix, Fig. S1*). Briefly, mice were entrained to a 12-h light/12-h dark (LD) cycle for 14 d, transferred to constant darkness (DD) for 24 h, and killed at circadian times (CT0, CT4, CT8, CT12, CT16, CT20, and CT24). Liver samples from two mice were collected and analyzed following established ribosome profiling protocols (24). We prepared ribosome profiling libraries and sequenced ~70 million reads per sample; this resulted in 25 to 45 million reads that could be mapped to mRNA (25) (*SI Appendix, Table S1*). Ribosome-protected fragments primarily aligned to the coding regions and 5' untranslated regions (5'UTRs) of the mRNA, with few reads mapping to the 3' untranslated region (3'UTR) (*SI Appendix, Fig. S2A*). Alignment of coding sequence (CDS)-mapped reads based on the footprint length revealed reading frame periodicity (*SI Appendix, Fig. S2B*). Reads were of the expected size, mapped with a high percentage to mRNA, and were correlated between samples (*SI Appendix, Fig. S2 C–E*).

From ~14,000 well-translated transcripts (defined by a median of at least two reads per five-codon mRNA window), we identified rhythms in ribosome-protected read fragments using the JTK_CYCLE algorithm (26), yielding 2,952 rhythmic transcripts with an adjusted $P < 0.05$, including well-known circadian transcripts such as *Bmal1*, *Per1*, *Per2*, *Clock*, and *Cry1* (*Dataset S1* and *SI Appendix, Table S2* and *Fig. S6A*).

Relationship between Ribosome Profiling Reads and Protein Levels.

We compared the timing of protein production, as measured by ribosome profiling reads, to the absolute number of protein molecules per cell for 16 previously reported core circadian proteins (10). There was broad agreement in the timing of ribosome binding compared to that of protein abundance (*Fig. 1A*). However, for several circadian proteins, such as BMAL1 and CLOCK, there was a delay of approximately 6 h between peak ribosome binding and peak protein abundance, clearly outside the 4-h range of our sampling intervals (*Fig. 1B*), which suggested that there is a posttranslational delay in protein turnover for these molecules rather than a posttranscriptional delay in ribosome binding. We compared the average number of ribosome profiling reads to the number of protein molecules over a 24-h period but found that the two values were poorly correlated (*Fig. 1C*). We measured this protein production efficiency (as defined by the ratio of our mass-spectrometry protein levels to ribosome profiling reads) at each time point. For some proteins, such as BHLHE40, a

large amount of ribosome binding resulted in a moderate amount of protein (*Fig. 1D*), whereas for other proteins, such as PER2, a much smaller amount of ribosome binding resulted in the same amount of protein as BHLHE40 (*Fig. 1E*), which suggests that BHLHE40 protein is more unstable than PER2 or that some other factor is limiting the amount of BHLHE40 produced. Thus, ribosome profiling reads can provide an approximate estimate for when a protein is produced, but protein abundance reflects both protein production and posttranslational mechanisms to control overall protein levels (27).

When we compared mRNA and protein abundance phases in our dataset in DD to the reported phases in previously published studies of mouse liver in LD (12, 15, 16, 18), we observed a correlation with a 1 to 2 h delay in DD (*SI Appendix, Fig. S10 A and C*). The transcripts with the largest differences in delay in the mRNA-to-peak-protein abundance between LD and DD conditions included *Nfil3*, *Per2*, *Per3*, and *Bmal1* (*SI Appendix, Fig. S10B*). The differences resulted from a slightly earlier peak in RNA abundance and ribosome binding in LD rather than a delay in the protein abundance peak; there was little difference between LD and DD in the delay between RNA abundance and ribosome binding (*SI Appendix, Fig. S10D*). Although these small differences may reflect a true biological effect from light-dependent changes in transcription, they could also simply result from differences in the algorithms used for phase determination, differences in experimental conditions, or both. Besides these 16 core circadian transcripts, most other transcripts with rhythmic ribosome binding in our dataset had a phase of around CT0 (*SI Appendix, Fig. S6*).

uORFs Suppress Translation. We also noticed a relationship between ribosome occupancy and the presence of uORFs, similar to previous reports (15, 18). Roughly half of all mouse transcripts contained at least one uORF (*SI Appendix, Fig. S4B*), and we found rhythmic ribosome binding in 602 uORFs with an adjusted $P < 0.05$ using JTK_cycle (*Dataset S2*). In particular, for circadian transcripts, such as *Cry1* and *Bmal1*, there appeared to be increased ribosome binding in uORF regions, as measured by increased ribosome profiling reads (*Fig. 2A*), although ribosome binding in the 5'UTR was not always associated with uORFs in circadian transcripts (*SI Appendix, Fig. S4A*). mRNAs with increased numbers of uORFs had lower levels of ribosome occupancy in the downstream CDS (*Fig. 2B*), whereas the length of the uORF and the distance of the uORF to the start codon did not have a significant impact on ribosome binding in the CDS (*SI Appendix, Fig. S4 C and D*). To investigate whether uORFs were sufficient to suppress translation in a combinatorial manner, we created a luciferase reporter vector with multiple synthetic uORFs. Predictably, increasing the number of uORFs reduced luminescence from the reporter (*Fig. 2C*). Using this synthetic reporter, we varied the position of a single uORF relative to the start codon or the uORF length and found a higher degree of uORF-mediated repression the closer the uORF was to the start codon; however, uORF length had no effect on repression (*SI Appendix, Fig. S4 E and F*). Both the position of the uORF and the number of uORFs altered the amplitude and mesor (mean luminescence) without altering the period using two different promoters in cell-based circadian luminescence assays (*SI Appendix, Fig. S15*). Other factors, such as the Kozak consensus of the uORF, overlap with the CDS, or uORF conservation may also impact repression strength (28, 29).

The *Per2* uORF Suppresses Reporter Expression without Altering Period. To further explore the impact of uORFs on circadian rhythms, we focused on the uORF in the circadian transcript

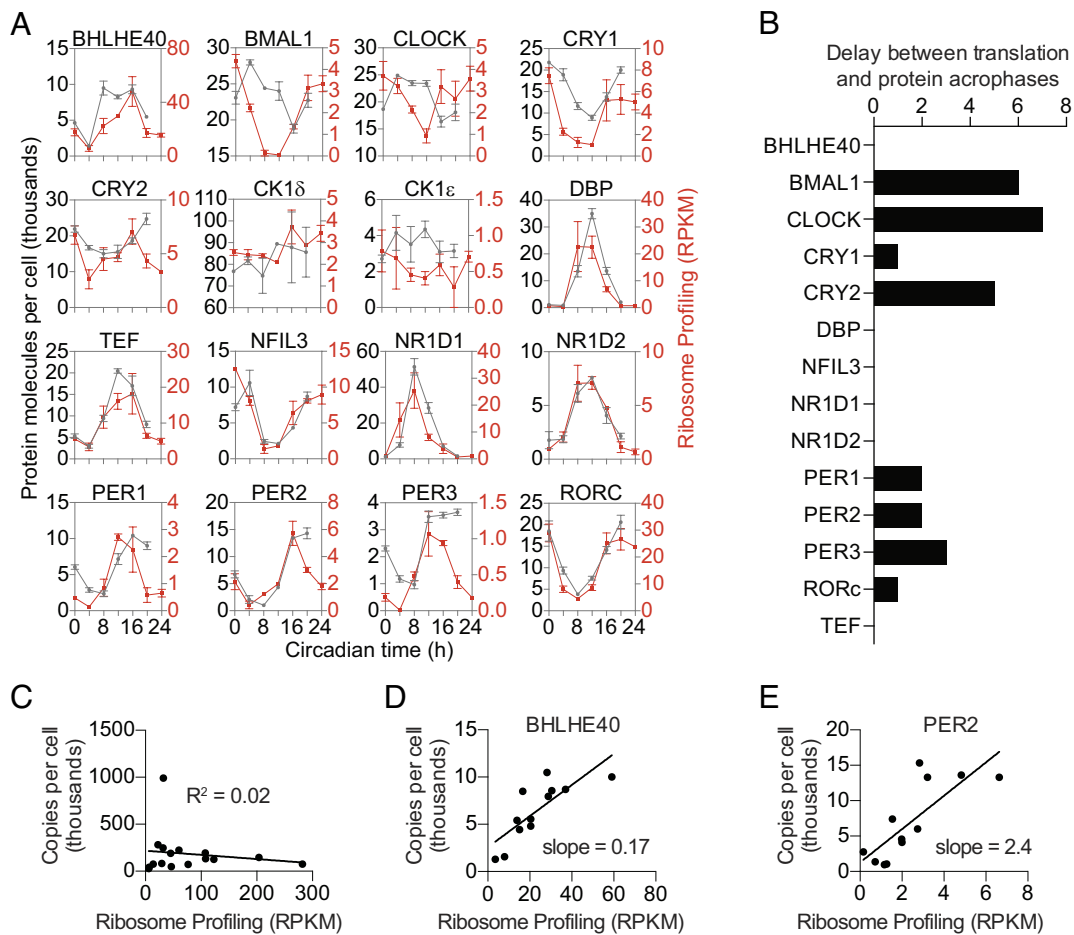


Fig. 1. Measuring translation and protein from the same liver samples for 16 circadian mRNAs. (A) Time course of the quantified proteins and the corresponding translation level. Protein concentration (gray) is expressed as copies per cell assuming that the total amount of protein per cell is 0.5 ng for the average for all quantified peptides (10). Ribosome binding (red) is expressed as reads per kilobase of transcript per million mapped reads (RPKM). Data are mean \pm SEM. (B) Phase delay between ribosome binding and protein abundance. Copies per cell were averaged from all peptides for each protein. JTK analysis was used to estimate the phases for these averaged protein levels and for ribosome binding RPKM levels. (C) Linear regression analysis comparing ribosome binding to protein amount averaged over 24 h showed that there was no correlation between ribosome binding and protein abundance (D and E) Linear regression analysis comparing ribosome binding to protein amount at each sampled time point showed that some proteins like BHLHE40 (D) had high protein turnover or reduced protein biosynthesis, whereas other proteins like PER2 (E) had low protein turnover or increased protein biosynthesis.

Per2. This uORF is evolutionarily conserved and consists of only a start and stop codon (Fig. 3A and *SI Appendix*, Fig. S13), which eliminates any potential effect of a translated uORF peptide on the regulation of *Per2*. Ribosomes bound the *Per2* uORF rhythmically and slightly before peak ribosome binding on the *Per2* transcript (Fig. 3B). Mutation of the uORF in *Per2* increased the amplitude of expression without affecting the phase or period in 3T3 cells transfected with a luminescence reporter (Fig. 3C and D). This increase in amplitude was not affected by the amount of transfected plasmid, inclusion of the full-length *Per2* 5'UTR, or addition of PER2 protein (*SI Appendix*, Fig. S5). CRISPR/Cas9-mediated mutation of the *Per2* uORF in PER::LUC MEFs increased overall luciferase expression levels compared to that of wild-type MEFs; however, we were unable to generate circadian rhythms in these cells to determine the impact of the *Per2* uORF on other circadian parameters such as period and phase (*SI Appendix*, Fig. S12).

To understand uORF-mediated repression in individual cells, we created a GFP fluorescent reporter plasmid driven by the *Per2* promoter with or without a mutation in the *Per2* uORF. We transfected 3T3 cells with these plasmids and an mCherry normalization plasmid and analyzed the cells by FACS (*SI Appendix*, Fig. S11). Mutation of the uORF increased GFP brightness without affecting mCherry brightness in individual cells (Fig. 3E), and increased the GFP-to-mCherry ratio of the population (Fig. 3F)

regardless of whether the cells were first gated on mCherry expression (Fig. 3E and F) or GFP expression (*SI Appendix*, Fig. S11C and D). Mutation of the uORF also increased the total number of GFP-expressing cells without affecting the total number of mCherry-expressing cells (Fig. 3G). Thus, the *Per2* uORF can repress reporter expression within individual cells to control circadian amplitude.

Mice with a Mutation in the *Per2* uORF have Reduced Sleep.

We used CRISPR/Cas9 to generate a knock-in mouse harboring a mutation in the uORF of *Per2*, which removed both the start and stop codon of the uORF without disrupting a nearby E'-box (*SI Appendix*, Fig. S7A). Wild-type and mutant mice were phenotyped over 13 d in LD and then for 12 d in DD using the Snappy Sleep Stager (30, 31), which is a respiration-based method to characterize sleep/wake parameters and circadian rhythms. Both male and female *Per2* uORF mutant mice had significantly reduced sleep per day (mean \pm SEM: 717 \pm 19 min and 642 \pm 7 min, respectively) compared to their wild-type littermates (774 \pm 11 min and 678 \pm 4 min, respectively, $P < 0.001$ by two-way ANOVA) and a corresponding increase in wake duration per day (Fig. 4A and B and *SI Appendix*, Fig. S8A) in LD conditions. There was a decrease in sleep episode duration and a significant increase in the transition probability from sleep to awake termed P_{sw} in *Per2*

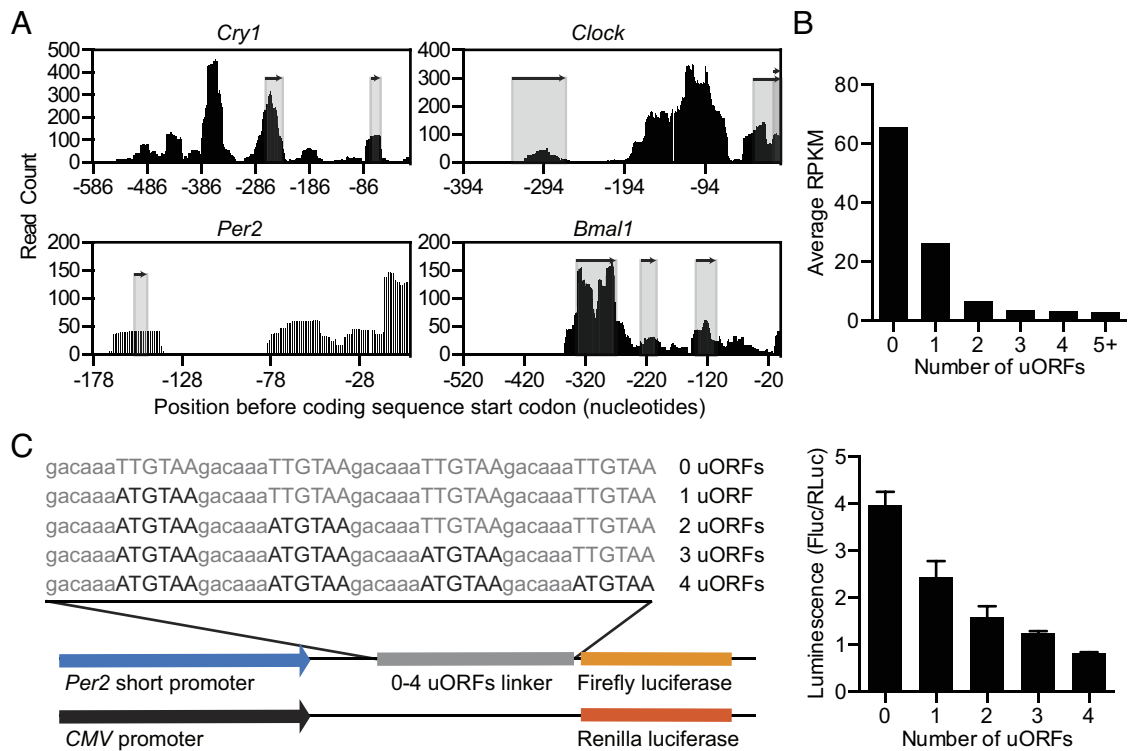


Fig. 2. uORFs suppress protein expression. (A) The 5'UTRs of *Cry1*, *Clock*, *Per2*, and *Bmal1* transcripts contain at least one uORF (shaded regions below arrows). The distribution of raw counts of ribosome profiling reads summed across all time points (black bars) for the 5'UTR of each transcript is shown. (B) Global distribution of uORFs compared to ribosome profiling translation level (RPKM) shows that mRNAs with more uORFs are translated less compared to mRNAs with fewer uORFs. (C) Introduction of a variable number of synthetic uORFs represses relative luminescence from a *Per2* short promoter in a dose-dependent manner.

uORF mutant mice (SI Appendix, Fig. S8B); however, there were no differences in other sleep parameters such as amplitude, P_{us} (the transition probability from awake to sleep), or wake episode duration (SI Appendix, Fig. S8C). *Per2* uORF mutant mice exhibited reduced sleep duration particularly during the light-to-dark and dark-to-light transitions in the early morning and early evening (Fig. 4 C and D). There were also differences in sleep duration later in the morning (SI Appendix, Fig. S8D) but not at other times during the day (SI Appendix, Fig. S8E). Next, we observed mice in constant darkness over 12 d and found no differences in activity rhythms or period (Fig. 4E); furthermore, there were less pronounced sleep differences in DD compared to LD (SI Appendix, Fig. S9). Cosinor analysis of the activity rhythms in LD and DD conditions revealed no differences in period and amplitude between wild-type and *Per2* uORF mutant mice (SI Appendix, Fig. S9).

To understand the molecular mechanisms behind these phenotypic differences, we performed ribosome profiling and total RNA sequencing of the liver from wild-type and *Per2* uORF mutant male mice killed at ZT02-04 (32) (SI Appendix, Figs. S18 and S19 and Datasets S4 and S5). Because *Per2* levels are near their lowest at ZT02-04, we hypothesized that this time point would show the largest difference in derepression of *Per2* by mutation of the *Per2* uORF. There was an increase in ribosome binding in *Per2* uORF mutant mice (SI Appendix, Fig. S19C), particularly in the 5'UTR and around the start codon (SI Appendix, Fig. S19 D and E). *Per2* RNA levels were also higher in the mutant mice by total RNA sequencing (SI Appendix, Fig. S19 C and H and Dataset S5) and confirmed by qPCR analysis (SI Appendix, Fig. S19B), although no differences were observed in *Per2* translation efficiency (TE), which is defined as the ratio of ribosome profiling reads to bulk RNA-seq reads (SI Appendix, Fig. S19G and Dataset S4). Protein levels were similar in *Per2* uORF mutant mice compared to that in wild-type mice (SI Appendix, Fig. S19

A and I). Taken together, these results suggest that *Per2* mRNA expression and ribosome binding is suppressed by the *Per2* uORF, which has a moderate impact on sleep duration.

Discussion

Global proteomics studies of mice livers revealed large numbers of diurnally rhythmic proteins. It has been estimated that 20 to 50% of these proteins are dependent on posttranscriptional and post-translational mechanisms (8, 9, 11, 12, 33). Previously, we used targeted proteomics to detect the rhythmicity and concentration of a select number of low-abundance core circadian proteins in constant darkness conditions (10). Here, we used ribosome profiling and quantitative mass spectrometry to understand the relationship between those circadian protein rhythms and mRNA translation.

We found a correlation between the timing of protein production, as measured by ribosome profiling, and peak protein abundance for most transcripts (Fig. 1). However, BMAL1 and CLOCK proteins had a delay between peak ribosome binding and protein levels (Fig. 1) caused by delayed protein turnover via posttranslational modification pathways (34), rather than a delay in ribosome binding (SI Appendix, Fig. S3). The peak protein abundance of PER and CRY is also slightly delayed relative to their peak mRNA abundance (10, 19, 20), and we found that this was also due to protein turnover rather than to a delay in ribosome binding (SI Appendix, Fig. S3), similar to previous ribosome profiling studies (15, 16, 18). There was a larger delay between the peak abundance of *Cry2* ribosome binding and CRY2 protein than that of *Cry1*, which may simply be a result of the lower amplitude of CRY2 rhythms.

We lacked the RNA-seq data needed to compute TE in our circadian samples, which limited our ability to determine how uORF features in 5'UTRs, such as number, length, and distance to CDS, alter translation efficiency. However, using the closest publicly

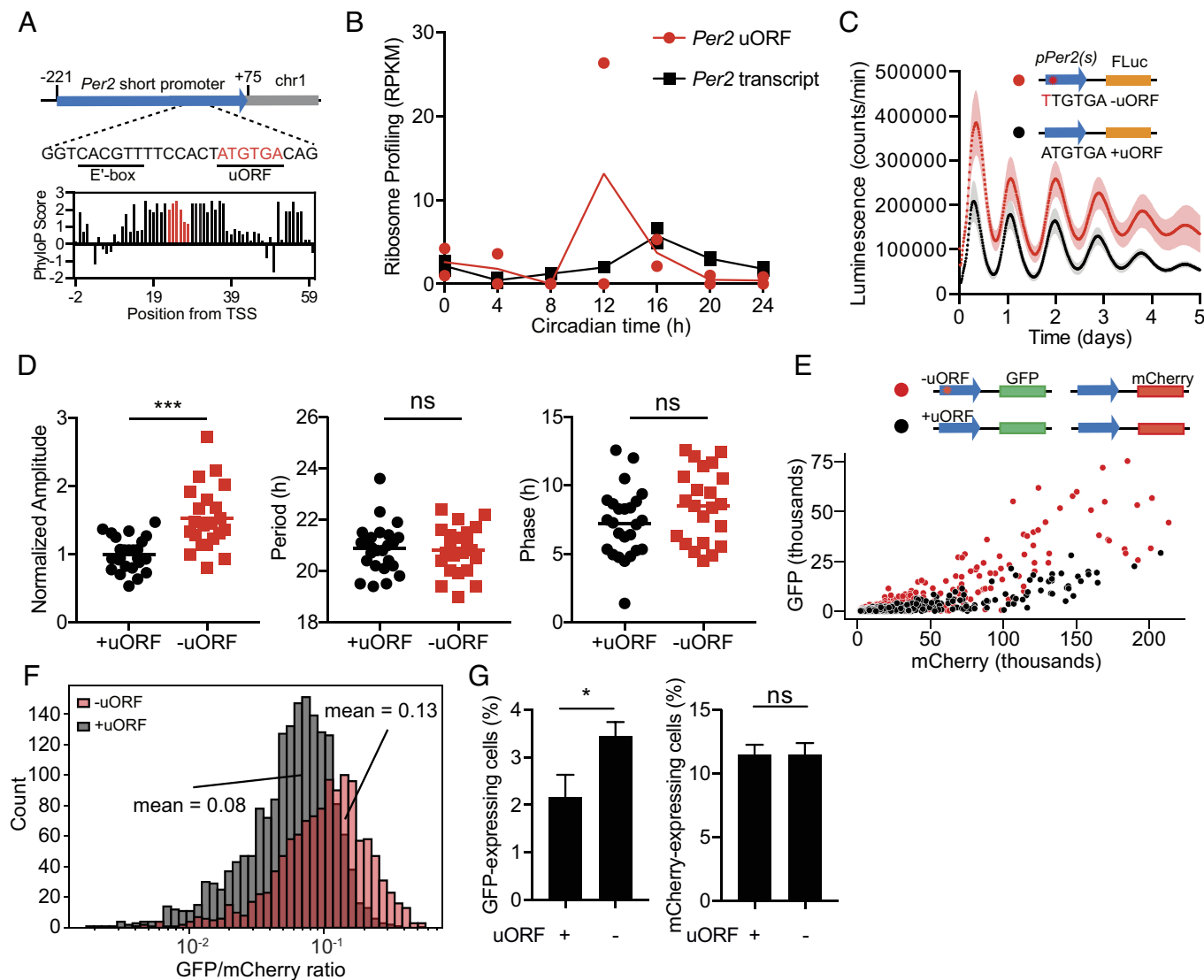


Fig. 3. The *Per2* uORF is evolutionarily conserved and suppresses PER2 expression. (A) Genomic position of the *Per2* short promoter, which contains an E'box and uORF. Evolutionary conservation scores according to UCSC genome browser among 22 mammalian species in the *Per2* 5'UTR (black bars) with the uORF highlighted (red bars). (B) Ribosome binding (RPKM) on the *Per2* uORF (red) compared to the *Per2* transcript (5'UTR, CDS, and 3'UTR, black). (C) Representative bioluminescent traces showing that mutation of the *Per2* uORF (ATGTAA to TTGTGA) increases the expression level of a pGL3-P(*Per2*)-dLuc luminescent reporter. Reporter containing uORF (black), reporter with a mutant uORF (red). The shaded region is SD. (D) Cosinor analysis showing the normalized amplitude (Left), period (Middle), and phase (Right) for cells transfected with the *Per2* uORF (black) or a mutant *Per2* uORF (red). Data from each group comprise at least 22 traces from eight different experiments (see *SI Appendix, Fig. S5*, for the plots of individual traces for each experiment). (E) Representative scatterplot of GFP versus mCherry expression for 3T3 cells transfected with a GFP-fluorescence reporter with a *Per2* uORF (+uORF, black) or a mutant *Per2* uORF (-uORF, red) and a mCherry-normalization plasmid. The analyzed cells were gated on mCherry+ expression. (F) Histogram of the GFP/mCherry ratio for cells in E. (G) The percentage of GFP+ cells (Left) was significantly higher in the -uORF population compared to the +uORF population, whereas the percentage of mCherry+ cells (Right) was unchanged ($n = 3$ independent experiments). See *SI Appendix, Fig. S11*, for FACS gating strategy and analysis of cells from the GFP+ gate.

available RNA-seq data (4) to our ribosome profiling data as a proxy for transcript abundance (Dataset S3), we observed a decrease in TE in transcripts with one or more uORFs (*SI Appendix, Fig. S16*), but no relationship between TE and uORF length or uORF distance to CDS (*SI Appendix, Fig. S17*).

Most transcripts with rhythmic translation in our dataset had a phase around CT0, corresponding to what would be the dark-to-light transition (*SI Appendix, Fig. S6*). Less than 10% of the circadian transcriptome had significant rhythms in mRNA abundance according to JTK cycle analysis ($P < 0.05$), and these transcripts were enriched for circadian and metabolic processes by Panther gene ontology (GO) analysis (*SI Appendix, Fig. S6 B and C*). Transcripts with a nonsignificant mRNA rhythmicity by JTK cycle analysis ($P > 0.05$) also were biased toward CT0, but there was no clear GO biological process underlying these rhythms

(*SI Appendix, Fig. S6 D and E*). The set of transcripts with phases between CT22 and CT02 (*SI Appendix, Fig. S6 F and G*) included *Npas2*, *Bmal1*, *Cry1*, *Nfil3*, and *Clock*. These transcripts are known to be regulated by the nuclear receptor NR1D1, also known as Rev-erb α , which transcriptionally represses many genes involved in metabolism in a tissue- and circadian-dependent manner (35). In the liver, NR1D1 predominantly binds genomic locations at ZT08-ZT10 with little-to-no binding at ZT22 (36–38). Thus, NR1D1 derepression may be driving some of transcriptional, and subsequent translational, peak observed in our data between CT22 and CT02. In addition, cyclic changes in translation machinery and polyadenylation (39, 40), translation activity of BMAL1 mediated by the mTORC1/S6K1 (41), or mTORC1 regulation by PER2 (42) may also drive rhythmic translation of nonrhythmic mRNA transcripts.

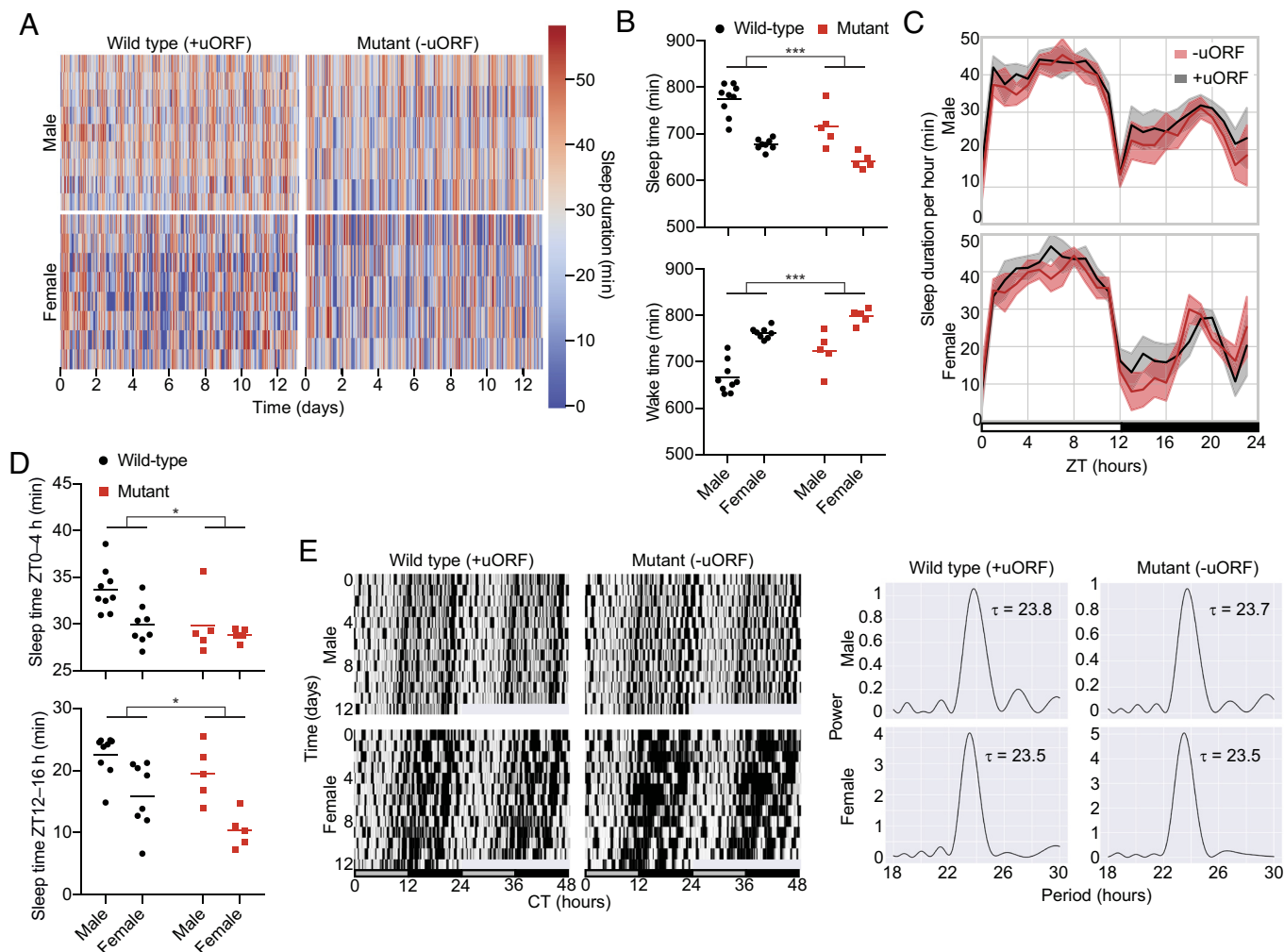


Fig. 4. Disruption of the *Per2* uORF reduces sleep in mice. (A) Sleep duration per hour over 13 d in 12-h light/12-h dark (LD) conditions for *Per2* uORF mutant and wild-type male and female mice. Each row indicates data from one mouse. (B) Mean sleep (Top) and wake (Bottom) duration over 24 h, averaged over 13 d. Red, *Per2* uORF mutant mice. Black, wild type. (C) Sleep duration per hour over 24 h in LD, averaged over 13 d for *Per2* uORF mutant (red) and wild-type (black) male (Top) and female (Bottom) mice. Lines indicate mean sleep duration at each time of day for each strain. Shaded area, SD at each time point. (D) Mean sleep duration per hour averaged over 13 d during the early morning (Top) and early evening (Bottom). *Per2* uORF mutant (red) and wild-type (black) dots are individual mice; lines indicate mean. (E) Representative double-plotted actograms of sleep duration per 6 min bins of wild-type and *Per2* uORF mutant mice in constant darkness (DD) over 12 d (Left) and corresponding periodograms (Right).

We observed widespread binding of ribosomes to uORFs in the 5'UTRs of many core circadian transcripts and found an inverse relationship between uORF number and luciferase expression in transiently transfected reporter cells and CRISPR/Cas9-generated MEF cells (Fig. 2 and *SI Appendix*, Figs. S4, S12, and S15). Approximately 50% of mouse and human mRNAs contain uORFs, which are associated with widespread translational repression (29). Thus, uORF-mediated suppression of translation may constitutively reduce the abundance of circadian proteins or provide a posttranscriptional foothold to adjust protein abundance by altering the activities of ribosome reinitiation factors (43–45). Moreover, mutagenesis of uORFs has been shown to alter rhythmicity in other circadian systems (46, 47). Not all ribosome binding in 5'UTRs was associated with uORFs, and we observed extensive ribosome binding in areas without an apparent uORF for *Cry1*, *Nr1d1*, *Clock*, *Dbp*, and *Per3* (Fig. 2 and *SI Appendix*, Fig. S4). For the *Nr1d1* 5'UTR, we observed close overlap in the nucleotides necessary for internal ribosome entry site (IRES)-mediated translation (48) and ribosome binding (*SI Appendix*, Fig. S14A) and confirmed IRES-mediated translation from the *Nr1d1* 5'UTR but not the *Cry1* 5'UTR (*SI Appendix*, Fig. S14B).

Near-cognate uORF translation (from a non-AUG start codon) may also drive ribosome binding (14). In silico mapping of near-cognate start codons with ribosome binding data revealed numerous potential near-cognate uORFs (*SI Appendix*, Fig. S14C) but experimental validation is still needed.

The uORF in the *Per2* 5'UTR is an attractive target to understand the role of uORFs in circadian biology, not only because cis-elements within the *Per2* promoter are well understood (49–52) but also because the *Per2* uORF is too short to encode a peptide. PER2 production is posttranscriptionally controlled by miRNAs (53, 54), antisense transcription (55), and hnRNP1-mediated mRNA degradation (56), which suggests that *Per2* posttranscriptional control is important for producing the optimal amount of PER2 protein. Mutation of the *Per2* uORF increased the amplitude of a reporter plasmid without affecting the phase or period (Fig. 3), similar to effects observed by mutating the *Per2* antisense transcript (57).

Both the abundance and timing of *Per2* expression are critical for maintaining circadian rhythmicity in mice because constitutive expression of PER2, unlike CRY1, disrupts behavioral rhythms (58). Several posttranscriptional mechanisms such as

Per2 antisense transcription (55) and miRNAs (53, 54, 59) in the *Per2* genomic locus alter the timing and abundance of PER2 protein expression. For example, replacing the *Per2* 3'UTR with an SV40 late poly(A) signal greatly amplifies bioluminescence rhythms in PER2:LUC mice and increases free-running periods (54). Mutation of the *Per2* uORF increased amplitude in reporter cells (Fig. 3) but did not increase the free-running period in mice (Fig. 4). *Per2* uORF mutant mice did have reduced total sleep in LD conditions (Fig. 4), as observed in *Per1/Per2* double mutant mice under similar sleep phenotyping conditions (30), but no significant change in sleep in DD conditions (SI Appendix, Fig. S9). Although our *Per2* mutation abolished the canonical ATGTGA uORF in the *Per2* 5'UTR, it also introduced a near-cognate uORF (CTGTAG) two nucleotides upstream of the original uORF. We think that this near-cognate uORF was non-functional because we observed increased *Per2* ribosome binding and mRNA levels in *Per2* uORF mutant mice compared to that in wild-type mice (SI Appendix, Fig. S19) and increased luciferase expression in mutant PER2:LUC MEF cells (SI Appendix, Fig. S12). One possible explanation for the rise in *Per2* mRNA levels is uORF-triggered nonsense-mediated decay (NMD) (60). In this scenario, mutation of the *Per2* uORF derepresses NMD of *Per2*, which results in an increase in *Per2* mRNA. However, *Per2* mRNA expression does not increase upon knockdown of the NMD component *Smg6* (61), which suggests that other proteins in NMD independent of SMG6 may be involved (62). Another group deleted the start codon of the *Per2* uORF but found no effect on *Per2* mRNA levels and did not perform ribosome profiling (63), so it is unclear whether ribosome binding in *Per2* is elevated in their *Per2* uORF mutant mice as it is in our mutant mice. In both studies, PER2 protein levels in the mutant mice were similar to that in wild-type mice, indicating that circadian proteostasis pathways compensate for the increase in PER2 protein production. In LD conditions, sleep in our *Per2* uORF mutant mice was particularly reduced during light-to-dark and dark-to-light transitions (Fig. 4), which may result from a lower sleep episode duration and an increase transition probability from sleep to wake (SI Appendix, Fig. S8B). Regulation of PER2 stability affects sleep (64, 65), and sleep deprivation reciprocally affects *Per2* expression (66–69) providing a rationale for how increased *Per2* expression could disrupt sleep in our mice. Mutation of the E' box cis-element, which is only a few base pairs upstream of the *Per2* uORF, abolishes molecular oscillations in mutant cells without disrupting the free-running period in mice (49). These mice re-entrain quicker under an artificial jetlag experiment than wild-type mice, and it will be interesting to observe how *Per2* uORF mutant mice behave under similar conditions. Further studies, particularly at a neurological level, are also needed to understand the precise mechanism by which sleep is reduced in these animals.

Materials and Methods

Animals. All animal experiments were approved by the Institutional Animal Care and Use Committee of the RIKEN Kobe branch. Eight-to-ten-week-old wild-type male mice (C57BL/6N, Japan SLC) were entrained under 12-h light (400 lx) 12-h dark (LD) for 2 wk. Twenty-four hours after transferring to constant darkness (DD), wild-type mice were killed every 4 h over one day (CT0, CT4, CT8, CT12, CT16, CT20, and CT24) for ribosome profiling analysis as in ref. 10. Livers were excised, snap-frozen in liquid nitrogen, and stored at -80°C until use. For details regarding *Per2* uORF mutant mouse construction, see SI Appendix.

Plasmids. For details regarding plasmid construction, see SI Appendix.

Ribosome profiling. Ribosome profiling was performed essentially as described in ref. 24. Frozen liver samples (~50 mg) were pulverized and then homogenized in 400 μL polysome lysis buffer (150 mM NaCl, 20 mM Tris-HCl pH 7.4, 5 mM

MgCl_2 , 5 mM DTT, 100 $\mu\text{g}/\text{mL}$ cycloheximide, 1% Triton X-100, and 25 U/mL Turbo DNase I). Lysates were incubated on ice for 5 to 10 min, triturated through a 26-G needle 10 times, and clarified by centrifugation (20,000 $\times g$ for 10 min at 4°C). About 300 μL of the supernatant was transferred to a new tube. Unbound RNA was digested by the addition of 7.5 μL RNase I (ThermoFisher) for 45 min and then stopped by 10 μL SUPERase In RNase Inhibitor (ThermoFisher). The digestion was transferred to 13 mm \times 51 mm polycarbonate ultracentrifuge tubes, layered on top of 0.9 mL sucrose cushion (150 mM NaCl, 20 mM Tris-HCl pH 7.4, 5 mM MgCl_2 , 5 mM DTT, 100 $\mu\text{g}/\text{mL}$ cycloheximide, 1 M sucrose, and 10 U/mL SUPERase In), and centrifuged in a TLA100.3 rotor at 70,000 rpm at 4°C for 4 h. Ribosome pellets were resuspended in 0.7 mL Qiazol, and mRNA was recovered using the miRNeasy RNA extraction kit (Qiagen) according to the manufacturer's instructions. For library construction and sequencing, see SI Appendix.

Bioinformatic analysis of ribosome profiling. For details regarding sequence processing and alignment, see SI Appendix. For each transcript, nonoverlapping five-codon windows were tiled across the coding region, and the transcript was considered well-translated if it had a median value of at least two reads per window (excluding the first fifteen and the last five codons). Using all well-translated transcripts, we created file where each transcript is represented across all samples by its RPKM value. We used this file in JTK_CYCLE (26) to identify all rhythmic transcripts. We used a threshold on the adjusted $P < 0.05$ to assess significance.

To detect uORFs, we processed the 5'UTR of all transcripts, extracted their sequence, and identified all pairs of a start codon (AUG) and a stop codon (UGA, UAA, or UAG) in phase with each other. Using the same read assignment method as in SI Appendix, we also allocated reads aligned to the UTR to their corresponding uORF (where appropriate).

Cells. NIH3T3 and MEFs from PER2::LUCIFERASE (PER2::LUC) knock-in reporter mice (70) were cultured in DMEM (ThermoFisher), 10% FBS (JRH Biosciences), and 1% penicillin/streptomycin (ThermoFisher) at 37°C in 5% CO_2 . For additional details, see SI Appendix.

Real-time circadian luciferase assay. Real-time circadian luciferase assays were performed as previously described (71). Briefly, the day before transfection, NIH3T3 cells or PER2:LUC MEFs were plated onto 35-mm dishes at a density 4×10^5 per well. The following day, NIH3T3 cells were cotransfected using FuGene6 (Roche) with 1 μg of the indicated luciferase reporter plasmid according to the manufacturer's instructions ($n = 3$) and cultured at 37°C . After 72 h, the media in the well were replaced with 2 mL of DMEM containing 10% FBS supplemented with 10 mM HEPES (pH 7.2, ThermoFisher), 0.1 mM luciferin (Promega), antibiotics, and 10 μM forskolin (Fermentek, NIH3T3) or 100 μM dexamethasone (ThermoFisher, PER2::LUC MEFs). Luminescence was measured by a photomultiplier tube (LM2400R, Hamamatsu Photonics) for 1 min at 12 min intervals in a darkroom at 30°C .

Dual-luciferase assay. NIH3T3 cells were plated on 6-well plates at a density of 2×10^5 per well. The following day cells were cotransfected with 0.95 μg of a Firefly luciferase reporter plasmid and 50 ng pHRL-SV40 plasmid (Renilla luciferase, Promega) as an internal control for transfection efficiency using FuGene6 (Roche). Cells were harvested and assayed by the Dual-Luciferase Reporter Assay System (Promega) according to the manufacturer's instructions 48 h after transfection.

Preparation of mouse nuclear lysate and immunoblot analysis. Mice were killed by cervical dislocation, and livers were dissected at CT2–4, snap-frozen in liquid nitrogen, and stored at -80°C . Liver extracts were prepared according to ref. 72 with minor modifications. See SI Appendix for further details.

FACS. NIH3T3 cells were plated onto plastic 35-mm dishes or 35-mm imaging dishes (Ibidi) at a density 4×10^5 per well. The following day, cells were cotransfected using FuGene6 (Roche) with 0.5 μg of the indicated fluorescence reporter plasmids (1 μg total) according to the manufacturer's instructions ($n = 3$) and cultured at 37°C . After 72 h, cells were trypsinized, sorted using FACS Aria I (BD Biosciences), and analyzed by FlowJo version 10.8.1.

Sleep phenotyping. Sleep phenotyping was conducted in 12-week-old (LD) and 14-week-old (DD) mice in a Snappy Sleep Stager (SSS) using *Per2* uORF mutant mice and wild-type littermates as a control (30). SSS is a noninvasive, respiration-based sleeping staging system in which mice are placed in a chamber connected to a respiration sensor that detects pressure differences between the outside and inside of the chamber. Detailed methods have been described previously (30). For details regarding sleep and wake parameters, see SI Appendix.

Statistical analyses. Statistical analyses were performed in R version 3.4.3, Prism 7.0, and custom Jupyter notebooks version 6.3. Two-way ANOVA and a Student's *t* test were used to test differences in sleep parameters between wild-type and *Per2* uORF mutant mice. For data analyzed by the Student's *t* test, the data were first confirmed to have a Gaussian distribution by the Shapiro-Wilk normality test, and equal variance within this distribution was confirmed by an F test. Lomb-Scargle periodograms were implemented using SciPy version 1.7, and cosinor analysis was implemented using CosinorPy (73). Statistical significance was defined as **P* < 0.05, ***P* < 0.01, ****P* < 0.001, and n.s. for not significant.

Data, Materials, and Software Availability. NGS data have been deposited in GEO (GSE201732 (25), GSE231820 (32)). Previously published data were used for this work [Data from mass spectrometry (Fig. 1A) and qPCR (SI Appendix, Fig. S3A) was previously published by our lab in Narumi et al., 2016 in PNAS.].

ACKNOWLEDGMENTS. We thank Ryohei Narumi for the circadian liver samples and for the use of the mass spectrometry and qPCR data and Dr. Shigehiro Kuraku and the Genome Information Research Center at Osaka University for sequencing of the ribosome profiling libraries. We thank Dr. Shihoko Kojima and Dr. Seung-Hee Yoo for PER2::LUC MEFs. We thank all lab members at the RIKEN Center for Biodynamics Research, in particular, Natsumi Hori and Yumika Sugihara for the production of mutant mice, and Masako Kunimi and Ruriko Inoue for breeding and helping with the phenotype measurements of the mutant mice. We thank all members of the Systems Immunology Laboratory and the Laboratory for Host Defense at the Immunology Frontier Research Center, in particular, Kitiya Piboonprai for help with genotyping and Shizuo Akira for his kind support. This work was also supported by grants from Exploratory Research

for Advanced Technology grant (JPMJER2001, H.R.U.) from the Japan Science and Technology Agency, KAKENHI Grant-in-Aid from the Japan Society for the Promotion of Science (Scientific Research S 18H05270 to H.R.U., Scientific Research C JP21K06385 to R.G.Y.), Human Frontier Science Program Research Grant Program (HFSP RGP0019/2018, H.R.U.), Ministry of Education, Culture, Sports, Science and Technology Quantum Leap Flagship Program (JPMXS0120330644), Japan Agency for Medical Research and Development (JP20am0401011), and the intramural Grant-in-Aid from the RIKEN Center for Biosystems Dynamics Research to H.R.U. This research was supported by the Research Support Project for Life Science and Drug Discovery (Basis for Supporting Innovative Drug Discovery and Life Science Research) from the Japan Agency for Medical Research and Development under Grant Number JP22ama121025. This work was supported by a Human Frontiers Science Program postdoctoral fellowship to A.M. and a Japan Society for the Promotion of Science Grant-in-Aid for Early Career Scientists (18K14755 to A.M.). Two children were born to A.M. during the course of this project, and he thanks them and Mari Nishino for their care, love, and support.

Author affiliations: ^aLaboratory for Synthetic Biology, RIKEN Quantitative Biology Center, Suita, Osaka 565-0871, Japan; ^bLaboratory for Host Defense, Immunology Frontier Research Center, Suita, Osaka 565-0871, Japan; ^cLaboratory for Systems Immunology, Immunology Frontier Research Center, Suita, Osaka 565-0871, Japan; ^dLaboratory of Animal Genetics and Breeding, Graduate School of Bioagricultural Sciences, Nagoya University, Nagoya 464-8601, Japan; ^eSchool of Computer Science, Queensland University of Technology, Brisbane QLD 4000, Australia; ^fCentre for Data Science, Queensland University of Technology, Brisbane QLD 4000, Australia; and ^gDepartment of Systems Pharmacology, Graduate School of Medicine, The University of Tokyo, Tokyo 113-0033, Japan

- J. A. Mohawk, C. B. Green, J. S. Takahashi, Central and peripheral circadian clocks in mammals. *Annu. Rev. Neurosci.* **35**, 445–462 (2012).
- A. Millius, H. R. Ueda, Systems biology-derived discoveries of intrinsic clocks. *Front. Neurol.* **8**, 25 (2017).
- R. A. Akhtar et al., Circadian cycling of the mouse liver transcriptome, as revealed by cDNA microarray, is driven by the suprachiasmatic nucleus. *Curr. Biol.* **12**, 540–550 (2002).
- N. Koike et al., Transcriptional architecture and chromatin landscape of the core circadian clock in mammals. *Science* **338**, 349–354 (2012).
- S. P. Gygi, Y. Rochon, B. R. Franza, R. Aebersold, Correlation between protein and mRNA abundance in yeast. *Mol. Cell. Biol.* **19**, 1720–1730 (1999).
- C. Lim, R. Allada, Emerging roles for post-transcriptional regulation in circadian clocks. *Nat. Neurosci.* **16**, 1544–1550 (2013).
- A. B. Reddy et al., Circadian orchestration of the hepatic proteome. *Curr. Biol.* **16**, 1107–1115 (2006).
- D. Mauvoisin et al., Circadian clock-dependent and -independent rhythmic proteomes implement distinct diurnal functions in mouse liver. *Proc. Natl. Acad. Sci. U.S.A.* **111**, 167–172 (2014).
- M. S. Robles, J. Cox, M. Mann, In-vivo quantitative proteomics reveals a key contribution of post-transcriptional mechanisms to the circadian regulation of liver metabolism. *PLoS Genet.* **10**, e1004047 (2014).
- R. Narumi et al., Mass spectrometry-based absolute quantification reveals rhythmic variation of mouse circadian clock proteins. *Proc. Natl. Acad. Sci. U.S.A.* **113**, E3461–3467 (2016).
- M. S. Robles, S. J. Humphrey, M. Mann, Phosphorylation is a central mechanism for circadian control of metabolism and physiology. *Cell Metab.* **25**, 118–127 (2017).
- J. Wang et al., Nuclear proteomics uncovers diurnal regulatory landscapes in mouse liver. *Cell Metab.* **25**, 102–117 (2017).
- N. T. Ingolia, S. Ghaemmaghami, J. R. S. Newman, J. S. Weissman, Genome-wide analysis in vivo of translation with nucleotide resolution using ribosome profiling. *Science* **324**, 218–223 (2009).
- N. T. Ingolia, L. F. Lareau, J. S. Weissman, Ribosome profiling of mouse embryonic stem cells reveals the complexity and dynamics of mammalian proteomes. *Cell* **147**, 789–802 (2011).
- C. Jang, N. F. Lahens, J. B. Hogenesch, A. Sehgal, Ribosome profiling reveals an important role for translational control in circadian gene expression. *Genome Res.* **25**, 1836–1847 (2015).
- F. Atger et al., Circadian and feeding rhythms differentially affect rhythmic mRNA transcription and translation in mouse liver. *Proc. Natl. Acad. Sci. U.S.A.* **112**, E6579–E6588 (2015).
- V. Castelo-Szekely, A. B. Arpat, P. Janich, D. Gatfield, Translational contributions to tissue specificity in rhythmic and constitutive gene expression. *Genome Biol.* **18**, 116 (2017).
- P. Janich, A. B. Arpat, V. Castelo-Szekely, M. Lopes, D. Gatfield, Ribosome profiling reveals the rhythmic liver transcriptome and circadian clock regulation by upstream open reading frames. *Genome Res.* **25**, 1848–1859 (2015).
- C. Lee, J. P. Etcheberry, F. R. Cagampang, A. S. Loudon, S. M. Reppert, Posttranslational mechanisms regulate the mammalian circadian clock. *Cell* **107**, 855–867 (2001).
- M. D. Field et al., Analysis of clock proteins in mouse SCN demonstrates phylogenetic divergence of the circadian clockwork and resetting mechanisms. *Neuron* **25**, 437–447 (2000).
- A. Honkela et al., Genome-wide modeling of transcription kinetics reveals patterns of RNA production delays. *Proc. Natl. Acad. Sci. U.S.A.* **112**, 13115–13120 (2015).
- Y. Liu, A. Beyer, R. Aebersold, On the dependency of cellular protein levels on mRNA abundance. *Cell* **165**, 535–550 (2016).
- Y. Shimizu et al., Cell-free translation reconstituted with purified components. *Nat. Biotechnol.* **19**, 751–755 (2001).
- N. T. Ingolia, G. A. Brar, S. Rouskin, A. M. McGeachy, J. S. Weissman, The ribosome profiling strategy for monitoring translation in vivo by deep sequencing of ribosome-protected mRNA fragments. *Nat. Protoc.* **7**, 1534–1550 (2012).
- Millius et al., Circadian ribosome profiling reveals a role for the Period2 upstream open reading frame in sleep. NCBI Gene Expression Omnibus (GEO). <https://www.ncbi.nlm.nih.gov/geo/query/acc.cgi?acc=GSE201732>. Deposited 22 April 2023.
- M. E. Hughes, J. B. Hogenesch, K. Kornacker, JTK_CYCLE: An efficient nonparametric algorithm for detecting rhythmic components in genome-scale data sets. *J. Biol. Rhythms* **25**, 372–380 (2010).
- S. Kojima, D. L. Shingle, C. B. Green, Post-transcriptional control of circadian rhythms. *J. Cell Sci.* **124**, 311–320 (2011).
- G.-L. Chew, A. Pauli, A. F. Schier, Conservation of uORF repressiveness and sequence features in mouse, human and zebrafish. *Nat. Commun.* **7**, 11663 (2016).
- T. G. Johnstone, A. A. Bazzini, A. J. Giraldez, Upstream ORFs are prevalent translational repressors in vertebrates. *EMBO J.* **35**, 706–723 (2016).
- G. A. Sunagawa et al., Mammalian reverse genetics without crossing reveals Nr3a as a short-sleeper gene. *Cell Rep.* **14**, 662–677 (2016).
- F. Tatsuki et al., Involvement of Ca(2+)-dependent hyperpolarization in sleep duration in Mammals. *Neuron* **90**, 70–85 (2016).
- Millius et al., Circadian ribosome profiling reveals a role for the Period2 upstream open reading frame in sleep. NCBI GEO. <https://www.ncbi.nlm.nih.gov/geo/query/acc.cgi?acc=GSE231820>. Deposited 5 May 2023.
- J. Wang et al., A proteomics landscape of circadian clock in mouse liver. *Nat. Commun.* **9**, 1553 (2018).
- Y. Okamoto-Uchida et al., Post-translational modifications are required for circadian clock regulation in vertebrates. *Curr. Genomics* **20**, 332–339 (2019).
- L. J. Everett, M. A. Lazar, Nuclear receptor Rev-erb α : Up, down, and all around. *Trends Endocrinol. Metab.* **25**, 586–592 (2014).
- D. Feng et al., A circadian rhythm orchestrated by histone deacetylase 3 controls hepatic lipid metabolism. *Science* **331**, 1315–1319 (2011).
- A. L. Hunter et al., Nuclear receptor REVERB α is a state-dependent regulator of liver energy metabolism. *Proc. Natl. Acad. Sci. U.S.A.* **117**, 25869–25879 (2020).
- Y. Zhang et al., Discrete functions of nuclear receptor Rev-erb α couple metabolism to the clock. *Science* **348**, 1488–1492 (2015).
- C. Jouffe et al., The circadian clock coordinates ribosome biogenesis. *PLoS Biol.* **11**, e1001455 (2013).
- F. Sirturel et al., Diurnal oscillations in liver mass and cell size accompany ribosome assembly cycles. *Cell* **169**, 651–663.e14 (2017).
- J. O. Lipton et al., The circadian protein BMAL1 regulates translation in response to S6K1-mediated phosphorylation. *Cell* **161**, 1138–1151 (2015).
- R. Wu et al., The circadian protein Period2 suppresses mTORC1 activity via recruiting Tsc1 to mTORC1 complex. *Cell Metab.* **29**, 653–667.e6 (2019).
- J. Bohlen et al., DENR promotes translation reinitiation via ribosome recycling to drive expression of oncogenes including ATF4. *Nat. Commun.* **11**, 4676 (2020).
- D. R. Morris, A. P. Geballe, Upstream open reading frames as regulators of mRNA translation. *Mol. Cell. Biol.* **20**, 8635–8642 (2000).
- S. Schleich et al., DENR-MCT-1 promotes translation re-initiation downstream of uORFs to control tissue growth. *Nature* **512**, 208–212 (2014).
- A. C. R. Dierfeller, T. Schafmeier, M. W. Mero, M. Brunner, Molecular mechanism of temperature sensing by the circadian clock of *Neurospora crassa*. *Genes Dev.* **19**, 1968–1973 (2005).

47. H.-W. Wu *et al.*, Noise reduction by upstream open reading frames. *Nat. Plants* **8**, 474–480 (2022).
48. D.-Y. Kim, K.-C. Woo, K.-H. Lee, T.-D. Kim, K.-T. Kim, hnRNP Q and PTB modulate the circadian oscillation of mouse Rev-erb alpha via IRES-mediated translation. *Nucleic Acids Res.* **38**, 7068–7078 (2010).
49. M. Doi *et al.*, Non-coding cis-element of Period2 is essential for maintaining organismal circadian behaviour and body temperature rhythmicity. *Nat. Commun.* **10**, 2563 (2019).
50. N. Gekakis *et al.*, Role of the CLOCK protein in the mammalian circadian mechanism. *Science* **280**, 1564–1569 (1998).
51. H. Hao, D. L. Allen, P. E. Hardin, A circadian enhancer mediates PER-dependent mRNA cycling in *Drosophila melanogaster*. *Mol. Cell. Biol.* **17**, 3687–3693 (1997).
52. H. R. Ueda *et al.*, System-level identification of transcriptional circuits underlying mammalian circadian clocks. *Nat. Genet.* **37**, 187–192 (2005).
53. I. Park *et al.*, microRNA-25 as a novel modulator of circadian Period2 gene oscillation. *Exp. Mol. Med.* **52**, 1614–1626 (2020).
54. S.-H. Yoo *et al.*, Period2 3'-UTR and microRNA-24 regulate circadian rhythms by repressing PERIOD2 protein accumulation. *Proc. Natl. Acad. Sci. U.S.A.* **114**, E8855–E8864 (2017).
55. R. A. Mosig *et al.*, Natural antisense transcript of Period2, Per2AS, regulates the amplitude of the mouse circadian clock. *Genes Dev.* **35**, 899–913 (2021).
56. K.-C. Woo *et al.*, Mouse period 2 mRNA circadian oscillation is modulated by PTB-mediated rhythmic mRNA degradation. *Nucleic Acids Res.* **37**, 26–37 (2009).
57. R. A. Mosig *et al.*, Natural Antisense Transcript of Period2, Per2AS, regulates the amplitude of the mouse circadian clock. *Genes Dev.* **35**, 899–913 (2020).
58. R. Chen *et al.*, Rhythmic PER abundance defines a critical nodal point for negative feedback within the circadian clock mechanism. *Mol. Cell* **36**, 417–430 (2009).
59. R. Nagel, L. Clijsters, R. Agami, The miRNA-192/194 cluster regulates the Period gene family and the circadian clock. *FEBS J.* **276**, 5447–5455 (2009).
60. J. A. Hurt, A. D. Robertson, C. B. Burge, Global analyses of UPF1 binding and function reveal expanded scope of nonsense-mediated mRNA decay. *Genome Res.* **23**, 1636–1650 (2013).
61. G. Katsioudi *et al.*, A conditional Smg6 mutant mouse model reveals circadian clock regulation through the nonsense-mediated mRNA decay pathway. *Sci. Adv.* **9**, eade2828 (2021)
62. V. Boehm *et al.*, SMG5-SMG7 authorize nonsense-mediated mRNA decay by enabling SMG6 endonucleolytic activity. *Nat. Commun.* **12**, 3965 (2021).
63. T. Miyake *et al.*, Minimal upstream open reading frame of Per2 mediates phase fitness of the circadian clock to day/night physiological body temperature rhythm. *Cell Rep.* **42**, 112157 (2023).
64. K. L. Toh *et al.*, An hPer2 phosphorylation site mutation in familial advanced sleep phase syndrome. *Science* **291**, 1040–1043 (2001).
65. K. Vanselow *et al.*, Differential effects of PER2 phosphorylation: Molecular basis for the human familial advanced sleep phase syndrome (FASPS). *Genes Dev.* **20**, 2660–2672 (2006).
66. J. P. Wisor *et al.*, A role for cryptochromes in sleep regulation. *BMC Neurosci.* **3**, 20 (2002).
67. T. Curie *et al.*, Homeostatic and circadian contribution to EEG and molecular state variables of sleep regulation. *Sleep* **36**, 311–323 (2013).
68. T. Curie, S. Maret, Y. Emmenegger, P. Franken, In vivo imaging of the central and peripheral effects of sleep deprivation and suprachiasmatic nuclei lesion on PERIOD-2 protein in mice. *Sleep* **38**, 1381–1394 (2015).
69. P. Franken, R. Thomason, H. C. Heller, B. F. O'Hara, A non-circadian role for clock-genes in sleep homeostasis: A strain comparison. *BMC Neurosci.* **8**, 87 (2007).
70. S.-H. Yoo *et al.*, PERIOD2::LUCIFERASE real-time reporting of circadian dynamics reveals persistent circadian oscillations in mouse peripheral tissues. *Proc. Natl. Acad. Sci. U.S.A.* **101**, 5339–5346 (2004).
71. M. Ukai-Tadenuma *et al.*, Delay in feedback repression by cryptochrome 1 is required for circadian clock function. *Cell* **144**, 268–281 (2011).
72. S. Masuda *et al.*, Mutation of a PER2 phosphodegron perturbs the circadian phosphoswitch. *Proc. Natl. Acad. Sci. U.S.A.* **117**, 10888–10896 (2020).
73. M. Moškon, CosinorPy: A python package for cosinor-based rhythmometry. *BMC Bioinformatics* **21**, 485 (2020).

Supporting Information for
Circadian ribosome profiling reveals a role for the *Period2* upstream
open reading frame in sleep.

Arthur Millius, Rikuhiko Yamada, Hiroshi Fujishima, Kazuhiko Maeda, Daron M. Standley,
Kenta Sumiyama, Dimitri Perrin, and Hiroki R. Ueda

Hiroki R. Ueda
Email: uedah-ky@umin.ac.jp

This PDF file includes:

Supporting text
Figures S1 to S21
Tables S1 to S3
Legends for Datasets S1 to S5
SI References

Other supporting materials for this manuscript include the following:

Datasets S1 to S5

1 Supporting Information Text

2 Methods

3 **Animals.** *Per2* uORF mutant (uORF: ATGTGA to mutant uORF: GTAGGT) mice were
4 generated by one-cell embryo microinjection of synthesized Cas9 mRNA, gRNA (5'-
5 TTTCCACTATGTGACAGCGGAGG-3'), and ssODN (5'-
6 GTCACGTTTTCCACTGTAGGTCAGCGGAGGGCGACG-3') in C57BL/6N fertilized
7 eggs, and genotypes were confirmed by Sanger sequencing.

8
9 **Plasmids.** The pGL3-P(*Per2*)-d*Luc* reporter plasmid (1) was modified by standard PCR
10 mutagenesis to generate pGL3-P(*Per2*)-uORF-d*Luc* (ATG->TTG mutation in the *Per2*
11 uORF). Synthetic oligonucleotide linkers containing 0-4 artificial uORFs (Fastmac, Japan)
12 were inserted into a PCR-linearized pGL3-P(*Per2*)-d*Luc* and pGL3-P(SV40)-3x*E'*box-d*Luc*
13 (2) by In-Fusion cloning (Takara Bio). Plasmids containing full-length *Per2* 5'UTR and
14 PER2 were cloned from mouse cDNA (Clone PX00938 H17, RIKEN) and pMU2-PER2-Luc
15 (3), respectively, and inserted into pGL3-P(*Per2*)-d*Luc* or pGL3-P(*Per2*)-uORF-d*Luc* by In-
16 Fusion cloning to create pGL3-P(*Per2*)-5'UTR-d*Luc* and pGL3-P(*Per2*)-5'UTR-PER2-d*Luc*
17 and the respective uORF mutant plasmids. Oligos for *Per2* sgRNA (5'-
18 caccgTTCCACTATGTGACAGCGGA and 5'-aacTCCGCTGTCACATAGTGGAac) were
19 annealed and inserted into *Bbs*I-digested pSpCas9(BB)-2A-Puro (Addgene #62988) or
20 pSpCas9n(BB)-2A-Puro (Addgene #62987) to make pCas9-*Per2* or pCas9n-*Per2*,
21 respectively. The promoter sequences from pGL3-P(*Per2*)-d*Luc* or pGL3-P(*Per2*)-uORF-
22 d*Luc* were cloned into pD1EGFP-N1 (Takara Bio) to create pD1-P(*Per2*)-EGFP or pD1-
23 P(*Per2*)-uORF-EGFP, respectively. mCherry was PCR-amplified and blunt-end ligated into
24 inverse-PCR amplified pD1-P(*Per2*)-EGFP for the mCherry version. The *Nr1d1* 5'UTR
25 (nucleotides 1-629 in NM_145434.4) and *Cry1* 5'UTR (nucleotides 1-583 in NM_007771.3)
26 were inserted into phpRL-BCL2-FL-pA (Addgene #42595) by In-Fusion cloning to create
27 phpRL-*Nr1d1* 5'UTR-pA and phpRL-*Cry1* 5'UTR-pA, respectively. All plasmid sequences
28 were verified by Sanger sequencing.

29
30 **Ribosome Profiling.** RNA was precipitated from the elution by the addition of 38.5 μ l water,
31 1.5 μ l GlycoBlue (ThermoFisher), and 10 μ l 3 M sodium acetate pH 5.5 followed by 150 μ l
32 isopropanol, stored overnight at -80 °C, pelleted by centrifugation (20,000 \times g for 30 min at
33 4 °C), and resuspended in 5 μ l 10 mM Tris pH 8. Approximately 2–4 μ g RNA was separated
34 on a 15% (wt/vol) polyacrylamide TBE-urea gel at 200 V for 65 min in 1 \times TBE, and
35 fragments between 26 and 34 nt were excised and recovered in 400 μ l RNA gel extraction
36 buffer (300 mM sodium acetate pH 5.5, 1 mM EDTA, and 0.25% (wt/vol) SDS) overnight.
37 RNA was precipitated by the addition of 1.5 μ l GlycoBlue and 500 μ l, stored at -80 °C for
38 >30 min, pelleted by centrifugation (20,000 \times g for 30 min at 4 °C), and resuspended in 10 μ l
39 10 mM Tris pH 8. RNA was dephosphorylated by T4 PNK (Takara Bio), precipitated and
40 recovered as previously described, resuspended in 8.5 μ l 10 mM Tris, and 1.5 μ l of
41 preadenylated and 3' blocked miRNA cloning linker
42 (1/5rApp/CTGTAGGCACCATCAAT/3ddC/, IDT) was added. The linker mixture was
43 denatured for 90 s at 80 °C, cooled to room temperature, ligated by T4 Rnl2 (NEB) for ~5 h
44 at room temperature, precipitated, recovered, and separated by 15% TBE-urea gel
45 electrophoresis. Ligation products were recovered overnight in RNA gel extraction buffer,
46 precipitated, and recovered in 10 μ l 10 mM Tris pH 8. Ligated RNA was reverse transcribed
47 at 48 °C for 30 min using SuperScript III (ThermoFisher) with the reverse transcription
48 primer (5'-(Phos)-
49 AGATCGGAAGAGCGTCGTGTAGGGAAAGAGTGTAGATCTCGGTGGTCGC-

1 (SpC18)-CACTCA-
2 (SpC18)- TTCAGACGTGTGCTCTTCCGATCTATTGATGGTGCCTACAG-3', where
3 SpC18 indicates a hexa-ethyleneglycol spacer). Reverse transcription products were
4 precipitated, recovered, separated by 15% TBE-urea gel electrophoresis, and recovered
5 overnight in DNA gel extraction buffer (300 mM NaCl, 10 mM Tris pH 8, and 1 mM
6 EDTA). The cDNA was precipitated, recovered, resuspended in 15 μ l 10 mM Tris pH 8, and
7 circularized by CircLigase (EpiCentre) for 1 h at 60 °C. rRNA was depleted by combining 5
8 μ l circularization reaction with 1 μ l of subtraction oligo pool, 1 μ l 20 \times SSC, and 3 μ l water,
9 incubating at 37 °C for 15 min and binding to MyOne Streptavidin C1 DynaBeads
10 (ThermoFisher) at 37 °C for 15 min with mixing at 1000 rpm. Eluate was precipitated,
11 recovered, and resuspended in 5 μ l 10 mM Tris pH 8. rRNA-depleted cDNA was PCR
12 amplified by Phusion High-Fidelity DNA Polymerase (NEB) in a 20 μ l reaction (denature
13 94 °C for 15 s, anneal 55 °C for 10 s, extend 72 °C for 10 s) for 12-16 cycles. PCR products
14 were separated on an 8% TBE gel, recovered overnight in DNA gel extraction buffer,
15 precipitated, recovered, and resuspended in 15 μ l 10 mM Tris pH 8. Libraries were quantified
16 using the high-sensitivity DNA chip on the Agilent BioAnalyzer according to the
17 manufacturer's protocol, pooled, and amplified on the Illumina HiSeq or NovaSeq6000
18 system according to the manufacturer's protocol.

19
20 **Bioinformatic analysis of ribosome profiling.** After quality control using FASTQC
21 (<https://www.bioinformatics.babraham.ac.uk/projects/fastqc/>), reads were clipped using
22 fastx_clipper (with parameters `-Q33 -a CTGTAGGCACCATCAAT -l 25 -c -n`) and
23 processed with fastx_trimmer (with parameters `-Q33 -f 2`), both from the FASTX-Toolkit
24 (http://hannonlab.cshl.edu/fastx_toolkit/). We then used Bowtie 2.1.0.0 (4) to map the
25 resulting reads to rRNA sequences. Reads that were successfully aligned to these sequences
26 are discarded, and only unaligned reads were used for downstream analysis. These reads that
27 did not align to rRNA were mapped to the mouse mm10 reference genome. Using samtools
28 0.1.19.0 and egrep, we extracted reads for which an exact match between the sequence and
29 the reference could be found.

30
31 Using reads aligned to a unique location, we then calculated transcript density profiles. This
32 relies on assignment each footprint alignment (i.e., each read) to a specific A site nucleotide
33 based on the length of the fragment. The initial assumption is that this site will be close to the
34 center of the read. To calculate the best offset, we considered a metagene that captured all
35 reads and their position relative to the start site and calculated the offset that optimized
36 phasing. The best results were obtained when the offset from the 5' end of the alignment was:
37 26 nt long, +13; 27-28 nt long, +15; 29-30 nt long, +16; 31-32 nt long, +17. Reads shorter
38 than 26 or longer than 32 nucleotides were discarded. Using this offset, we assigned each
39 read to a unique nucleotide, and constructed transcript density profiles by counting the
40 number of reads whose A site was assigned to each nucleotide position. Raw data has been
41 deposited in GEO (GSE201732 and GSE231820).

42
43 **Cells.** PER2::LUC MEFs were plated in 10 cm dishes at a density 4×10^5 per well,
44 transfected the next day with pCas9-Per2 or pCas9n-Per2 and 560 bp of single-stranded
45 linearized DNA (Guide-it Long ssDNA Production System, Takara Bio) containing
46 mutations in the Per2 uORF (ATGTGA to GTAGGT), and after 48-h selected in 1 μ g/ml
47 puromycin for puromycin-resistant clones according to (5). Individual clones were expanded,
48 sequence-verified, and clones containing at least one allele with a mutation in the Per2 uORF
49 were used for downstream analysis.

50

1 **Preparation of wild-type and *Per2* uORF mutant mouse lysate for ribosome profiling,**
2 **total RNA sequencing, qPCR, and immunoblot analysis.** Approximately 0.1 g mouse liver
3 tissue from wild-type and *Per2* uORF mutant male mice sacrificed at ZT02-04 was washed
4 repeatedly in ice-cold PBS (Nacalai), resuspended in 1 ml polysome lysis buffer (150 mM
5 NaCl, 20 mM Tris-HCl pH 7.4, 5 mM MgCl₂, 5 mM DTT, 100 µg/ml cycloheximide, 1%
6 Triton X-100, 25 U/ml Turbo DNase I), and homogenized by glass Dounce
7 microhomogenizer (>10 strokes tip A, then >10 strokes tip B). The homogenate was clarified
8 by centrifugation (20,000 × g for 10 min at 4 °C) and the supernatant divided – 300 µl was
9 immediately used for ribosome profiling library preparation as above, 200 µl was added to 1
10 mL TRIzol (Nacalai) for total RNA sequencing, and the remaining was snap frozen and
11 stored at -80 °C for subsequent western blot and qPCR analysis. Total RNA was extracted
12 and analyzed using the Agilent 2100 bioanalyzer according to the manufacturer's
13 instructions. Total RNA libraries were prepared using the TruSeq stranded mRNA kit
14 (Illumina) according to the manufacturer's instructions.

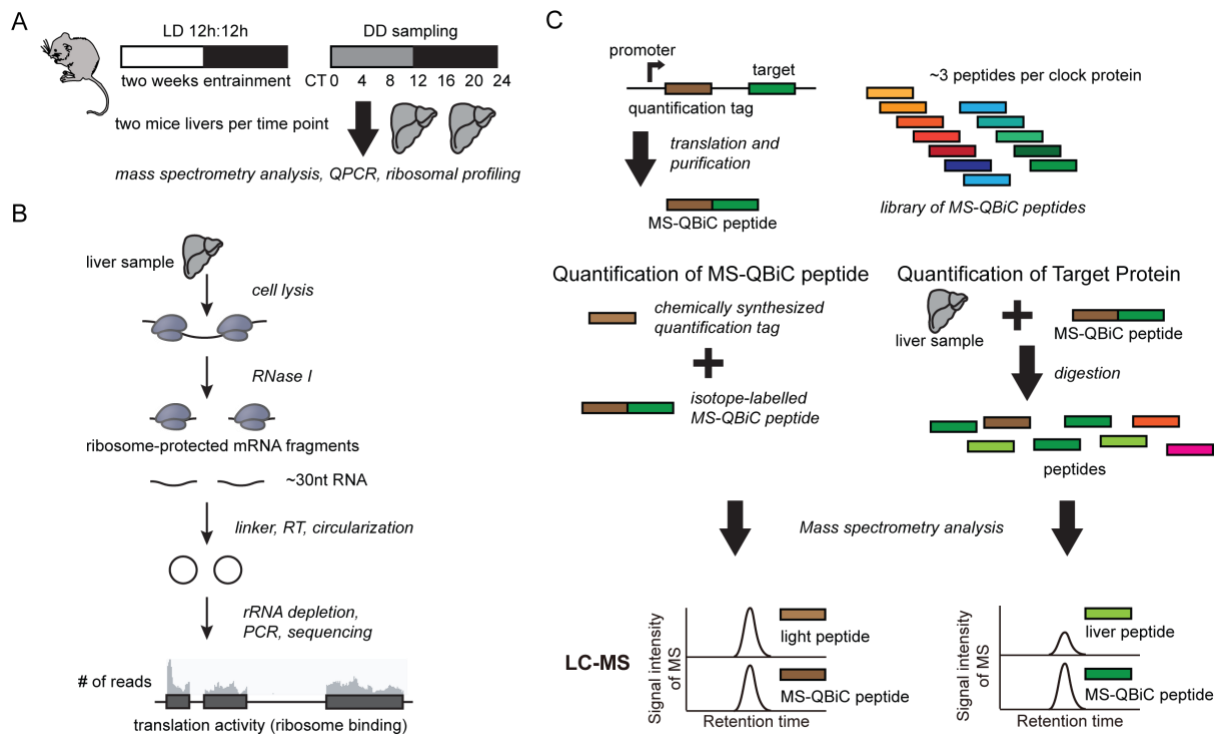
15
16 **Preparation of nuclear and cytoplasmic extracts.** Extracts were prepared essentially as
17 described previously (6) with some modifications. Approximately 0.1 g mouse liver tissue
18 from wild-type and *Per2* uORF mutant male mice sacrificed at ZT02-04 was washed
19 repeatedly in ice-cold PBS (Nacalai), resuspended in 1 ml per 0.1 g tissue in homogenization
20 buffer (5 mM KCl, 10 mM Tris-HCl pH 7.4, 2 mM EDTA, 1 mM DTT, 1× cComplete Mini
21 EDTA-free protease inhibitor tablet [Sigma]) + 2.2 M sucrose, and homogenized by glass
22 Dounce microhomogenizer (>10 strokes tip A, then >10 strokes tip B). Approximately 550 µl
23 lysate was layered on 1.5 ml sucrose cushion (homogenization buffer + 2.2 M sucrose + 10%
24 glycerol) in 13 mm × 51 mm polycarbonate ultracentrifuge tubes, and centrifuged in a
25 TLA100.3 rotor at 70,000 rpm at 4 °C for 45 min. The supernatant was removed and used as
26 the cytoplasmic extract. The nuclear pellet was rinsed once glycerol without disturbing the
27 pellet with homogenization buffer + 10% glycerol, then resuspended in 150 µl
28 homogenization buffer + 10% glycerol, transferred to a new tube containing 150 µl urea
29 buffer (2 M urea, 600 mM NaCl, 50 mM Tris pH 7.4, 1 mM DTT, 1× cComplete Mini EDTA-
30 free protease inhibitor tablet [Sigma]), incubated on ice for 20 min with occasional mixing,
31 and then centrifuged (20,000 × g for 10 min at 4 °C). This supernatant was used as the
32 nuclear extract.

33
34 **Western blot.** Total protein lysates were thawed and diluted to ~10 mg/ml in polysome lysis
35 buffer. Cytoplasmic and nuclear lysates were diluted to 1 mg/ml and 0.6 mg/ml, respectively,
36 in homogenization buffer + 10% glycerol. Lysates were separated by SDS-PAGE, transferred
37 to nitrocellulose membrane (ThermoFisher) by semidry transfer (Bio-Rad), blocked in 5%
38 (wt/vol) skim milk in TBST (50 mM Tris pH 7.5, 140 mM NaCl, 0.1% Tween) for 1 h at
39 22 °C, and then incubated overnight at 4 °C in anti-PER2 antibody (1:1000, PM083, Medical
40 & Biological Laboratories) or anti-histone H3 antibody (1:1000, 9715, Cell Signaling). After
41 washing in TBST, blots were incubated in anti-rabbit IgG HRP-conjugated secondary
42 antibody (1:2000, NA934, Cytivia) or mouse beta-actin conjugated-HRP antibody (0.8:2000,
43 sc-47778, Santa Cruz Biotechnology) for 1 h at 22 °C and developed by Immobilon Forte
44 Western HRP (Millipore).

45
46 **qPCR.** Approximately 100 µl lysate was extracted in 1 ml TRIzol (Nacalai) according to the
47 manufacturer's instructions and re-suspended in 50 µl 10 mM Tris pH 8.0. RNA was digested
48 with TURBO DNaseI (ThermoFisher) for 1 h at 37 °C and recovered with an equal volume
49 1:1 phenol:chloroform containing isoamyl alcohol pH 5.2 (Nacalai). After centrifugation
50 (20,000 × g for 5 min at 4 °C), approximately 37.5 µl of the aqueous layer was precipitated

1 with 10 μ l 3 M sodium acetate pH 5.5 and 1.5 μ l GlycoBlue followed by 150 μ l isopropanol.
2 Samples were frozen at -80 $^{\circ}$ C for >30 min, centrifuged (20,000 \times g for 30 min at 4 $^{\circ}$ C),
3 washed in 500 μ l 75% ethanol, dried for 10 min at 37 $^{\circ}$ C, and RNA was resuspended in 15 μ l
4 10 mM Tris pH 8.0. Approximately 500 ng RNA was reverse transcribed using ReverTra
5 Ace qPCR RT Master Mix (Toyobo) and amplified using Thunderbird SYBR qPCR mix
6 (Toyobo) with *Per2* (forward: 5'-GCACATCTGGCACATCTCGG-3'; reverse: 5'-
7 TGGCATCACTGTTCTGAGTGTC-3') and *actin* (forward: 5'-
8 CACTGTCGAGTCGCGTCCA-3'; reverse: 5'-CATCCATGGCGAACTGGTGG-3') primers
9 on ViiA 7 (Applied Biosystems). Relative *Per2* mRNA was quantified using the $\Delta\Delta$ CT
10 method with *actin* as a reference gene.

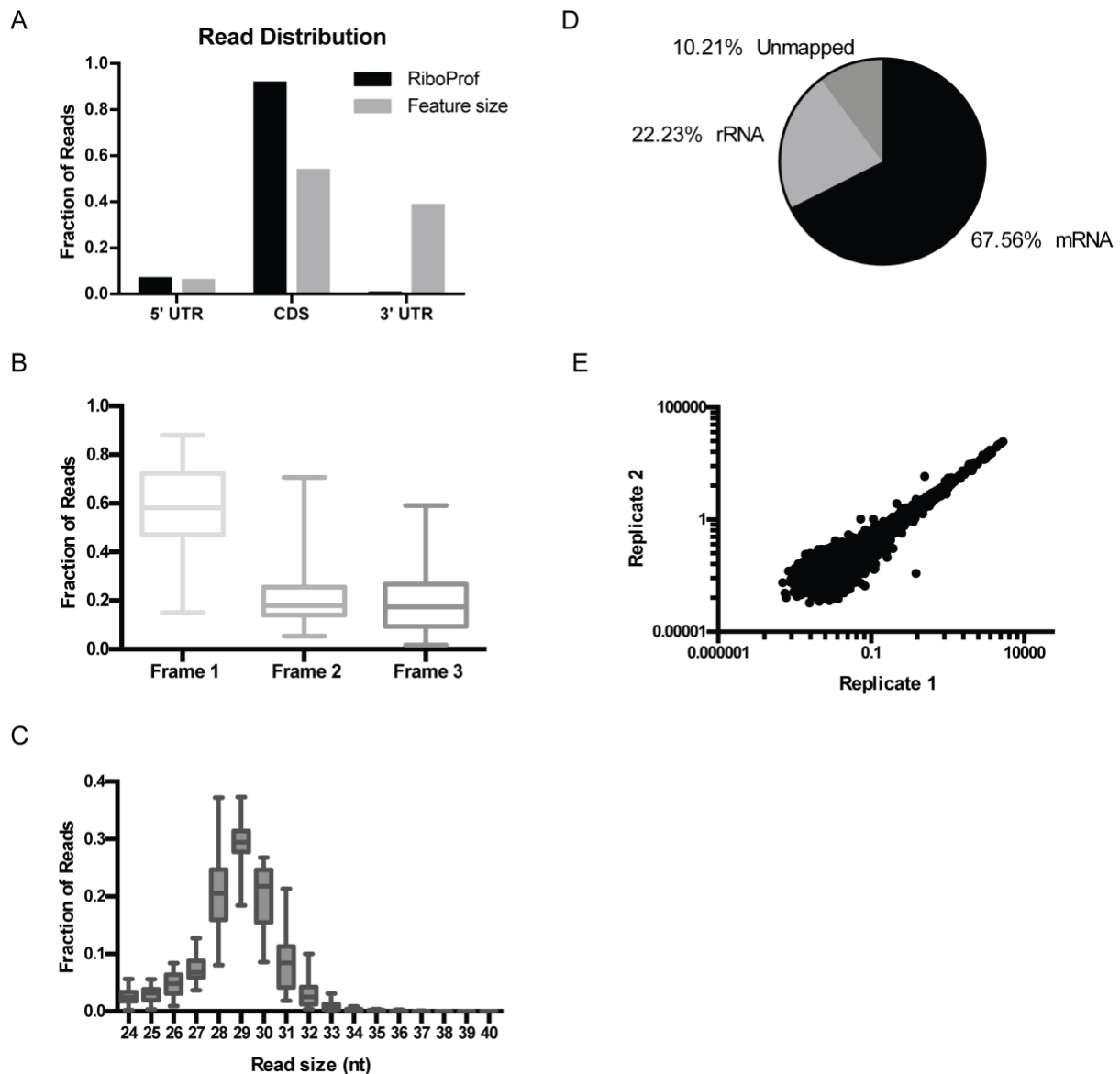
11
12 **Sleep and wake parameters.** Sleep and wake duration are the mean total sleep and wake
13 duration, respectively, per day over 13 d. P_{sw} is the transition probability from sleep to
14 awake; P_{ws} is the transition probability from awake to sleep. Mathematically, E_i is the i -th
15 epoch, which is either sleep (s) or wake (w). Let N_{XY} ($X, Y \in \{w, s\}$) be the number of elements
16 of the set $\{(E_i, E_{i+1}) \mid E_i = X, E_{i+1} = Y\}$. P_{ws} and P_{sw} are defined as $N_{ws}/(N_{ws} + N_{ww})$ and
17 $N_{sw}/(N_{sw} + N_{ss})$, respectively. The amplitude is defined as the coefficient of variation of sleep
18 time for each 10-min bin over 24 h.



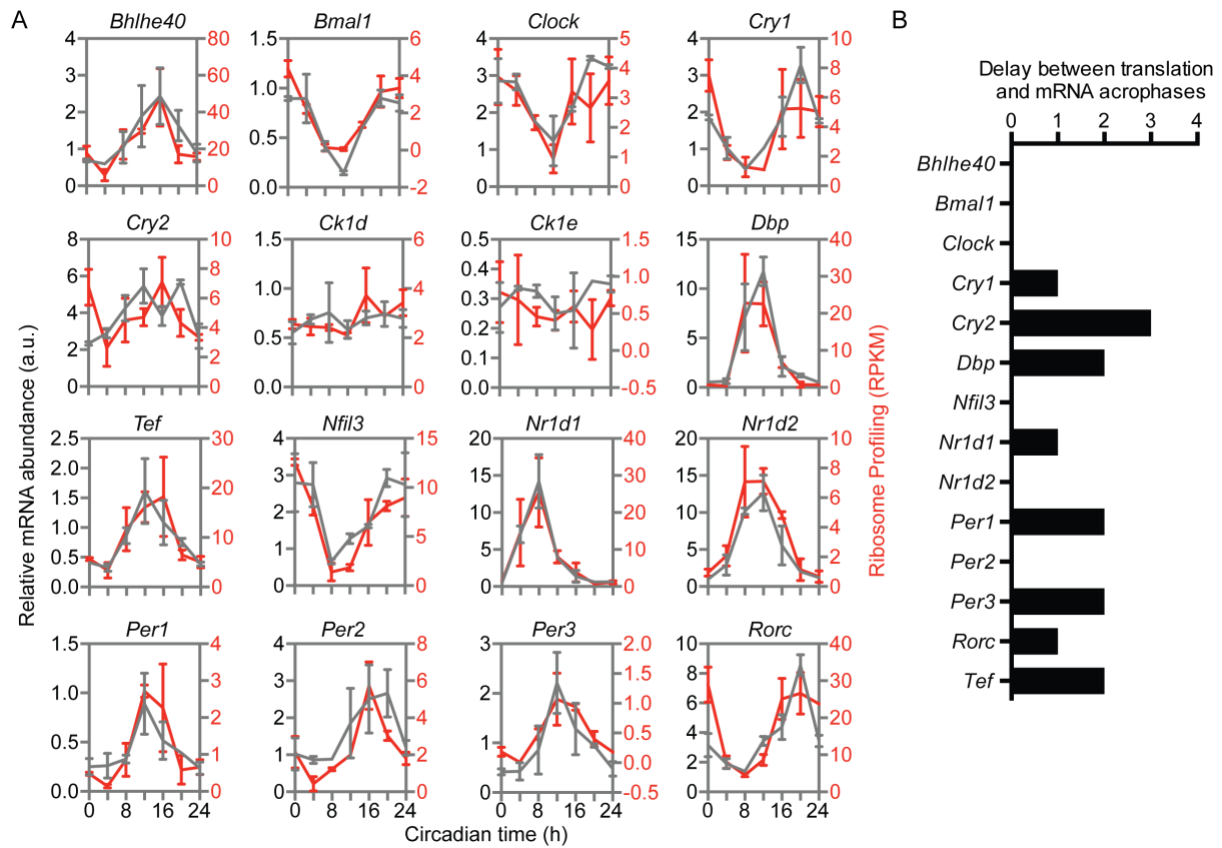
Supplementary Figure 1 | Analyzing mRNA expression, translation activity, and absolute protein copy number levels in the same mice liver samples over the course of a day (related to Figure 1).

(A) All mice were carefully kept and handled according to the RIKEN Regulations for Animal Experiments. Eight to ten-week-old-male mice (C57BL/6N, Japan SLC) were entrained under a 12–12 h light-dark (LD) conditions (400 lux) for 2 weeks. After transferring to constant darkness (DD), mice were sacrificed every 4 h over 1 day (i.e. CT0, 4, 8, 12, 16, and 20) for proteomic analyses, every 4 h over 1 day (i.e. CT0, 4, 8, 12, 16, 20, and 24) for ribosome profiling analyses, or every 4 h over 2 days (i.e. CT0, 4, 8, 12, 16, 20, 24, 28, 32, 36, 40, and 44) for qPCR analyses. (B) Two mice livers at seven different circadian time points were lysed and ribosomes were isolated by a sucrose cushion. Ribosome-protected mRNA fragments were extracted, reverse transcribed, and circularized into a library. Libraries were depleted of the common most abundant rRNA, PCR amplified and sequenced (~1.02 billion reads). (C) Schematic description of the MS-QBiC workflow. A purification-tag, a quantification-tag, and a tryptic peptide of the target protein (target peptide) were sequentially arrayed as a single peptide sequence (MS-QBiC peptide). The target peptide sequence was attached by one- or two-step PCR. The MS-QBiC peptide was synthesized in the PURE system in the presence of stable isotope-labeled Arg and Lys for isotopic labeling both the quantification-tag and the target peptide. Trypsin digestion of purified MS-QBiC peptide produced equal amounts of isotopically labeled quantification-tag

- 1 and target peptide. The quantification-tag was used to measure purified MS-QBiC peptide
- 2 and the target peptide was used as an internal standard for target protein quantification.



1
2 **Supplementary Figure 2 | Validation of ribosome profiling cDNA libraries (related to**
3 **Figure 1).** (A) Read distribution within 5'UTRs, CDS, and 3'UTRs compared with the size of
4 those features. Ribosome profiling reads are enriched for the CDS and 5'UTR, and relatively
5 few reads map to the 3'UTR. (B) Frame analysis of ribosome profiling reads of single protein
6 isoform mRNAs shows a preference for frame 1 (the coding frame). Box-and-whisker plots:
7 midline, median; box, 25th and 75th percentiles. Whiskers are minimum and maximum
8 values. (C) Box and whisker plots show the distribution of read lengths from all sequences.
9 The majority of reads were between 27 and 32 nt, which matches the footprint size of the
10 ribosome. (D) Summary of mapped reads. (E) Correlation of RPKM between replicate 1 and
11 replicate 2 at CT0 shows a high degree of correlation in ribosome binding between samples.



1
2
3
4
5
6
7
8
9

Supplementary Figure 3 | Measuring translation and RNA expression from the same

liver samples for 16 circadian mRNAs (related to Figure 1). (A) Time course of the

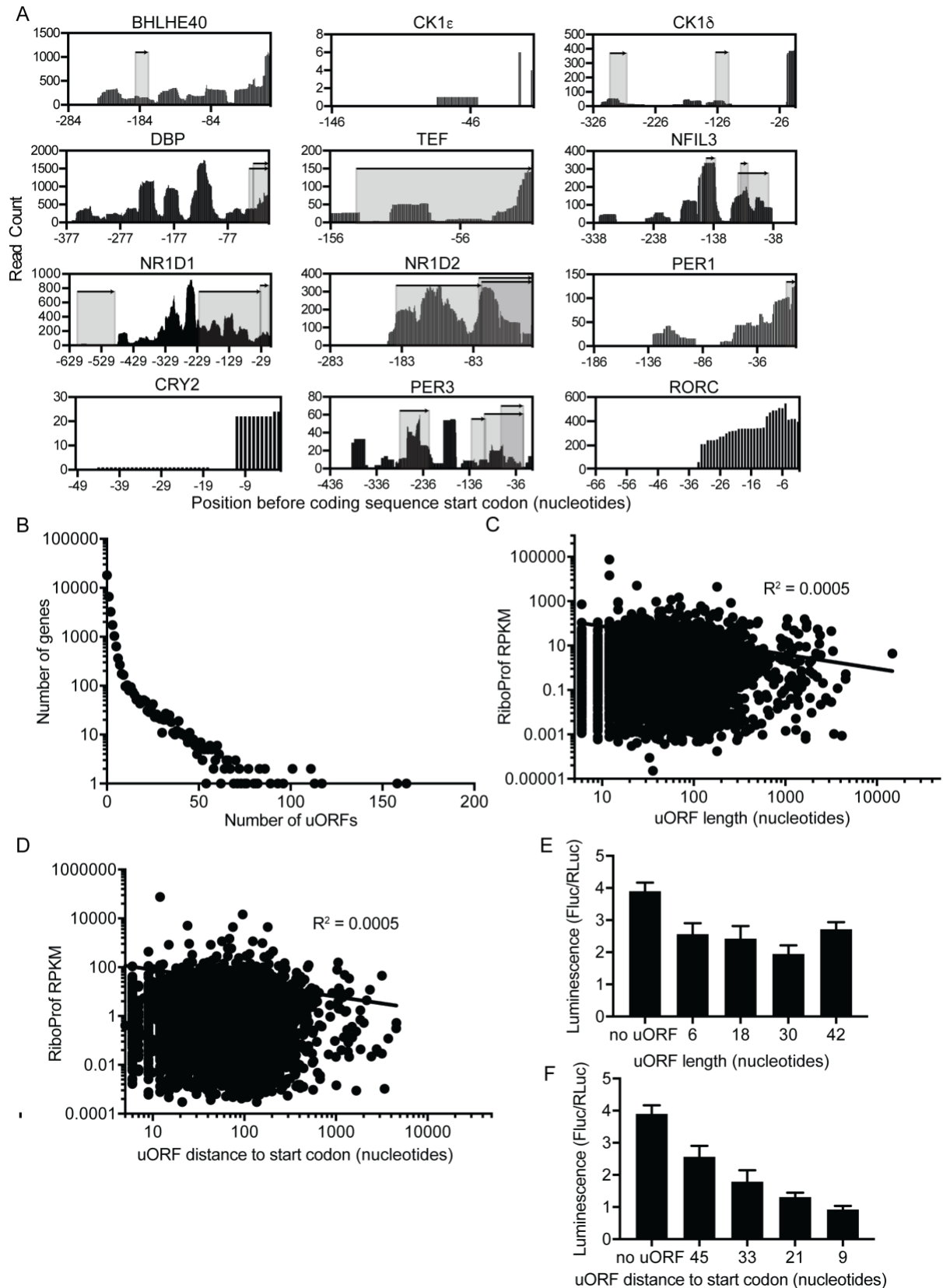
quantified RNA expression levels (grey) by qPCR derived from data in (7) and the

corresponding ribosome binding (RPKM, red). Error bars are the standard deviation of the

two replicates. (B) Phase delay between mRNA expression and ribosome binding. Absolute

cDNA abundance was calculated using the standard curve obtained from mouse genomic

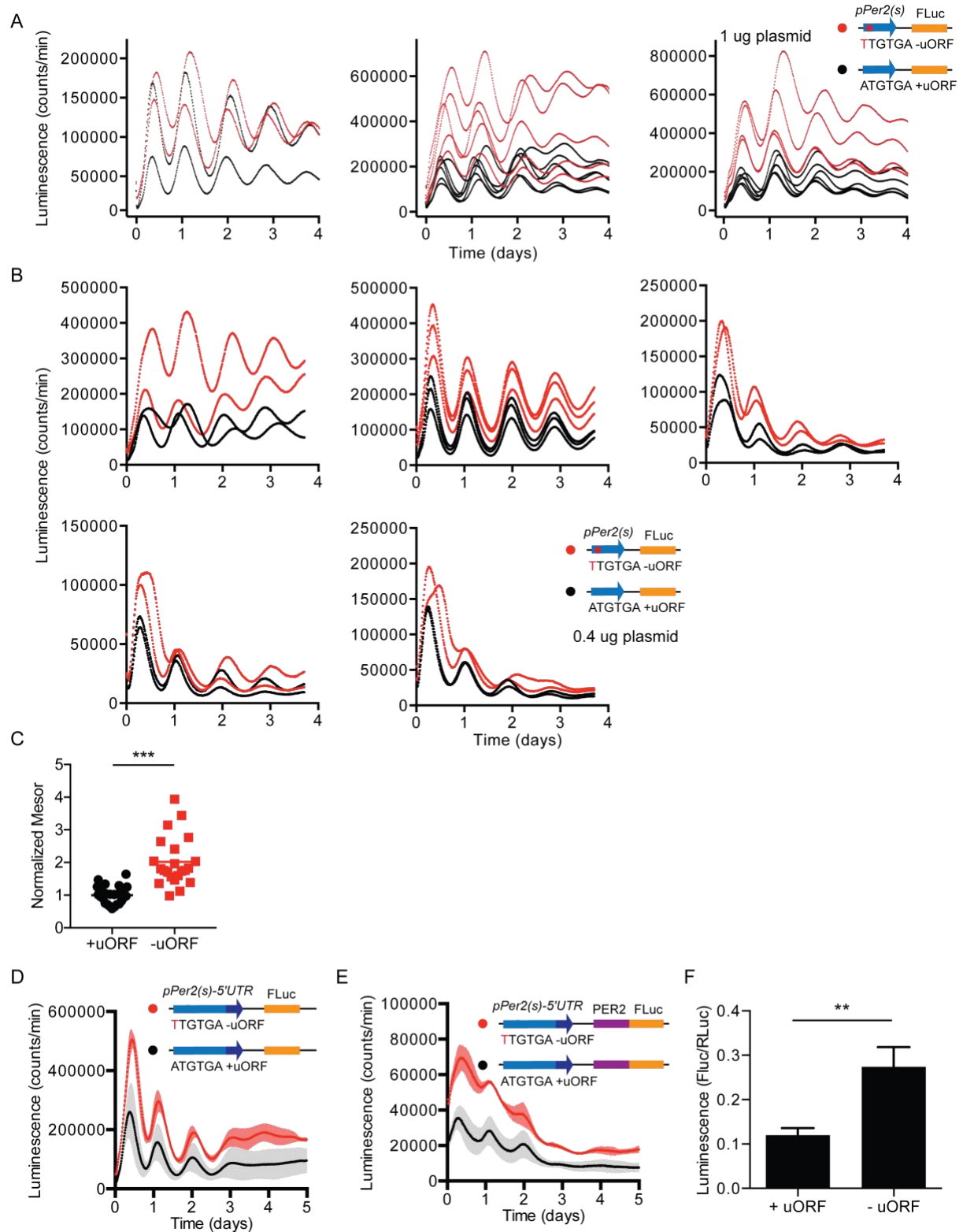
DNAs, and JTK analysis was used to estimate the phase of each mRNA.



1

2 **Supplementary Figure 4 | Distribution of upstream open reading frames in clock**
 3 **transcripts (related to Figure 2).** (A) The 5' UTRs of *Bhlhe40*, *Ck1ε*, *Ck1δ*, *Dbp*, *Tef*, *Nfil3*,
 4 *Nr1d1*, *Nr1d2*, *Per1*, *Cry2*, *Per3*, and *Rorc* transcripts, location of uORFs (shaded regions),

1 and raw read counts from the ribosome profiling data (black bars). **(B)** The number of
2 transcripts with a given number of uORFs. **(C)** The relationship between the length of an
3 uORF and ribosome binding (RPKM) in the corresponding ORF. **(D)** The relationship
4 between the distance of an uORF to the ORF start codon and ribosome binding (RPKM) in
5 the corresponding ORF. **(E)** Introduction of a single uORF in the *Per2* short promoter of
6 different lengths does not alter the relative luminescence of the *Per2* luciferase reporter. **(F)**
7 The distance of a single uORF in the *Per2* short promoter to the start codon correlates with
8 the relative luminescence of the *Per2* luciferase reporter.
9



1

2 **Supplementary Figure 5 | Detailed analysis of the *Per2* uORF (related to Figure 3). (A)**

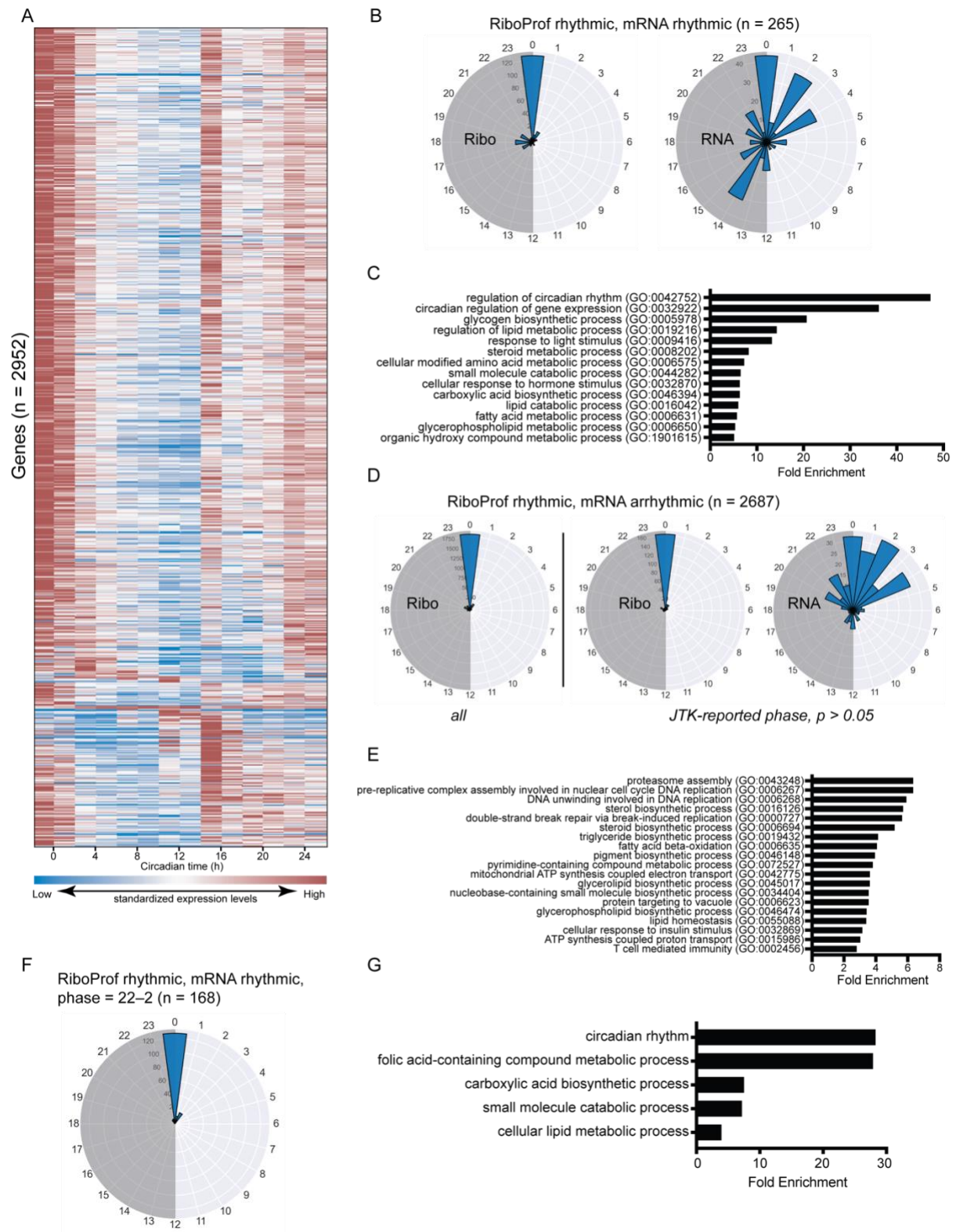
3 Bioluminescent recording of 3T3 cells transfected with the *Per2* short promoter containing a

4 wild-type (black) or mutant (red) *Per2* uORF at 1 µg (A) and 0.4 µg (B) transfected plasmid.

5 Each graph is an independent experiment performed on a different day; multiple traces on the

6 same graph indicate different transfected plates. Data from the upper middle panel of (B) was

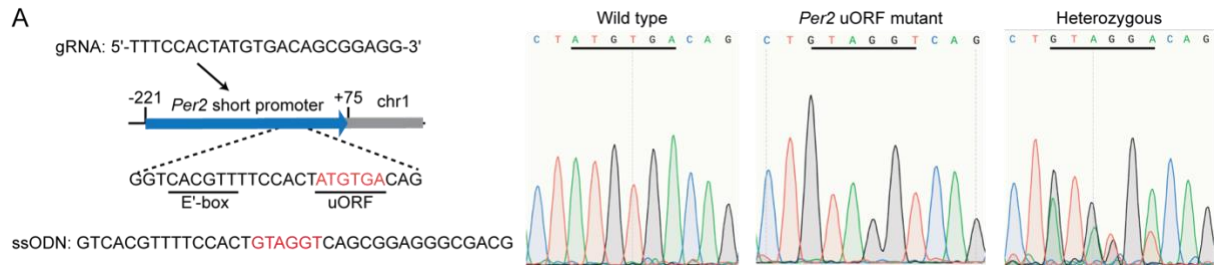
1 used for Fig. 3B. **(C)** Cosinor analysis showing normalized mesor for the bioluminescent
2 traces in **(A)** and **(B)**. **(D)** Mutation of the *Per2* uORF (ATGTAA to TTGTGA) with the full-
3 length *Per2* 5' UTR (red) increases the luminescence expression level of the reporter as
4 measured by bioluminescent recording compared to that of a reporter containing the uORF
5 (black). Shaded region is SD. **(E)** Mutation of the *Per2* uORF (ATGTAA to TTGTGA) with
6 the full-length *Per2* 5' UTR and PER2 protein (red) increases the luminescence expression
7 level of the reporter as measured by bioluminescent recording compared to that of a reporter
8 containing the uORF (black). Shaded region is SD. **(F)** Relative luminescence experiments of
9 3T3 cells transfected with (+uORF) or without (-uORF) the uORF in pGL3-P(*Per2*)-dLuc.
10



1

2 **Supplementary Figure 6 | Phase analysis (related to Figure 3).** (A) Heat map of ribosome
 3 profiling rhythmic transcripts identified by JTK cycling analysis ($P < 0.05$) showing RPKM
 4 data over 24 hours for 2952 genes. Transcripts are sorted by phase, and RPKM values are
 5 normalized within each gene (row). Note that most transcripts peak at CT0 (red bars in first
 6 two columns). (B) Polar histogram showing the ribosome profiling (*left*) and RNA (*right*)

1 phase distribution of the 265 ribosome profiling rhythmic and mRNA rhythmic transcripts.
2 **(C)** Panther analysis of gene ontology biological processes based on genes in **(B)** showing an
3 increase in circadian rhythm regulation pathways and metabolic processes. **(D)** Polar
4 histogram showing the ribosome profiling phase distribution (*left*) of the 2687 ribosome
5 profiling rhythmic transcripts that did not reach significance in mRNA rhythmicity.
6 Ribosome profiling (*middle*) and RNA (*right*) polar histograms for transcripts with an mRNA
7 JTK-reported phase $P > 0.05$ are also shown. **(E)** Panther analysis of gene ontology
8 biological processes based on the 2687 genes in **(D)**. **(F and G)** There were 168 transcripts
9 from **(B)** with a phase distribution between CT22-CT0 **(F)** corresponding to circadian rhythm
10 and metabolism processes by Panther analysis **(G)**. Note that this group includes NR1D1-
11 regulated transcripts including *Npas2*, *Arntl*, *Cry1*, *Nfil3*, and *Clock*.
12



1

2 **Supplementary Figure 7 | Disruption of the *Per2* uORF in mice (related to Figure 4). (A)**

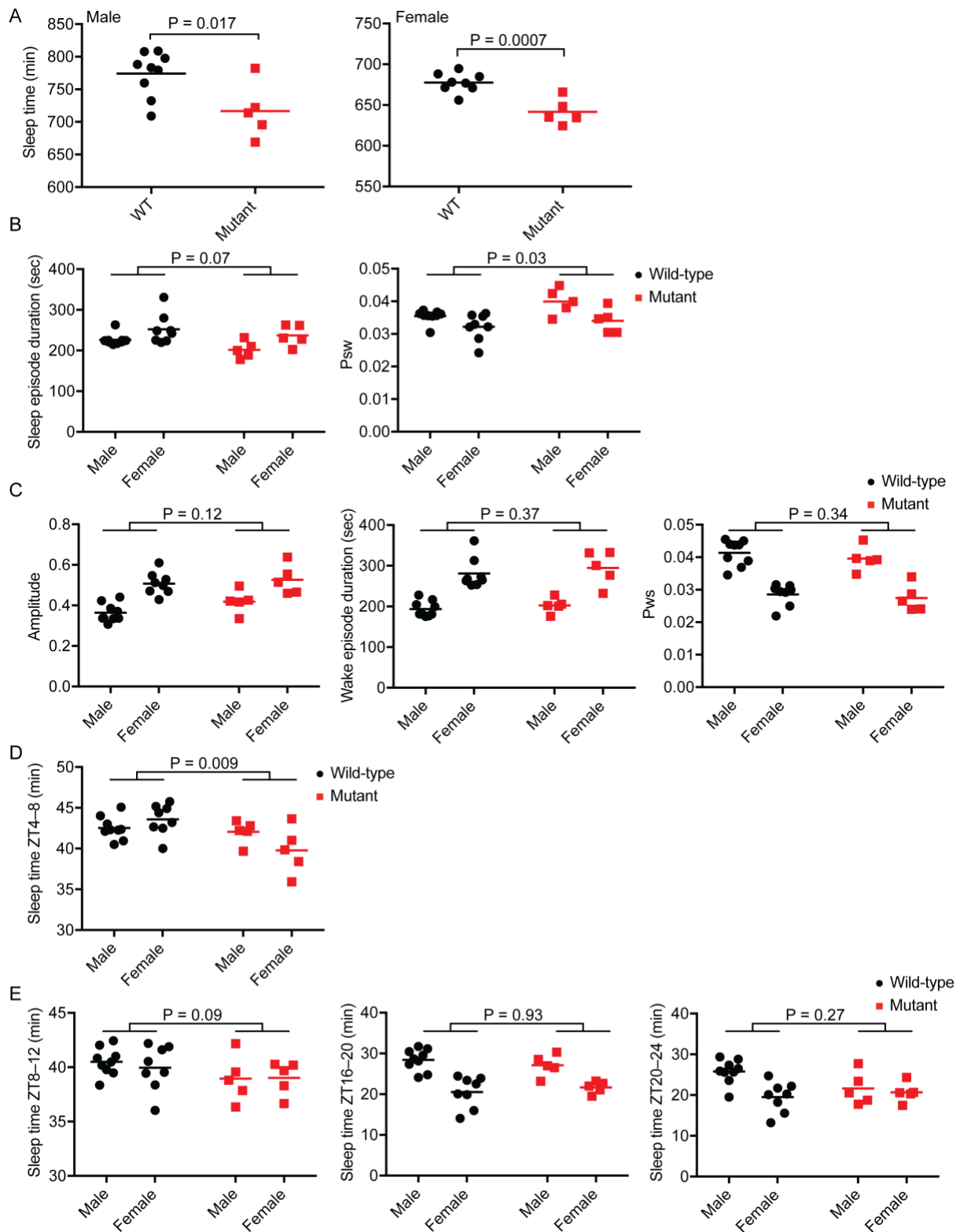
3 An ssODN replaced the *Per2* uORF (ATGTGA) with a mutant version (GTAGGT) in which

4 both the start and stop codons were mutated. The diagram shows the location of the CRISPR

5 gRNA and upstream E'box within the *Per2* promoter region (*left*). Representative Sanger

6 sequencing results from wild-type, *Per2* uORF mutant, and heterozygous mice are shown

7 (*right*).



1

2

Supplementary Figure 8 | Detailed analysis of 12 h light:12 h dark (LD) sleep

3

parameters (related to Figure 4). (A) Mean sleep duration over 24 h averaged over 13 d for

4

male (*left*) and female (*right*) mice. Red, *Per2* uORF mutant mice. Black, wild-type. P

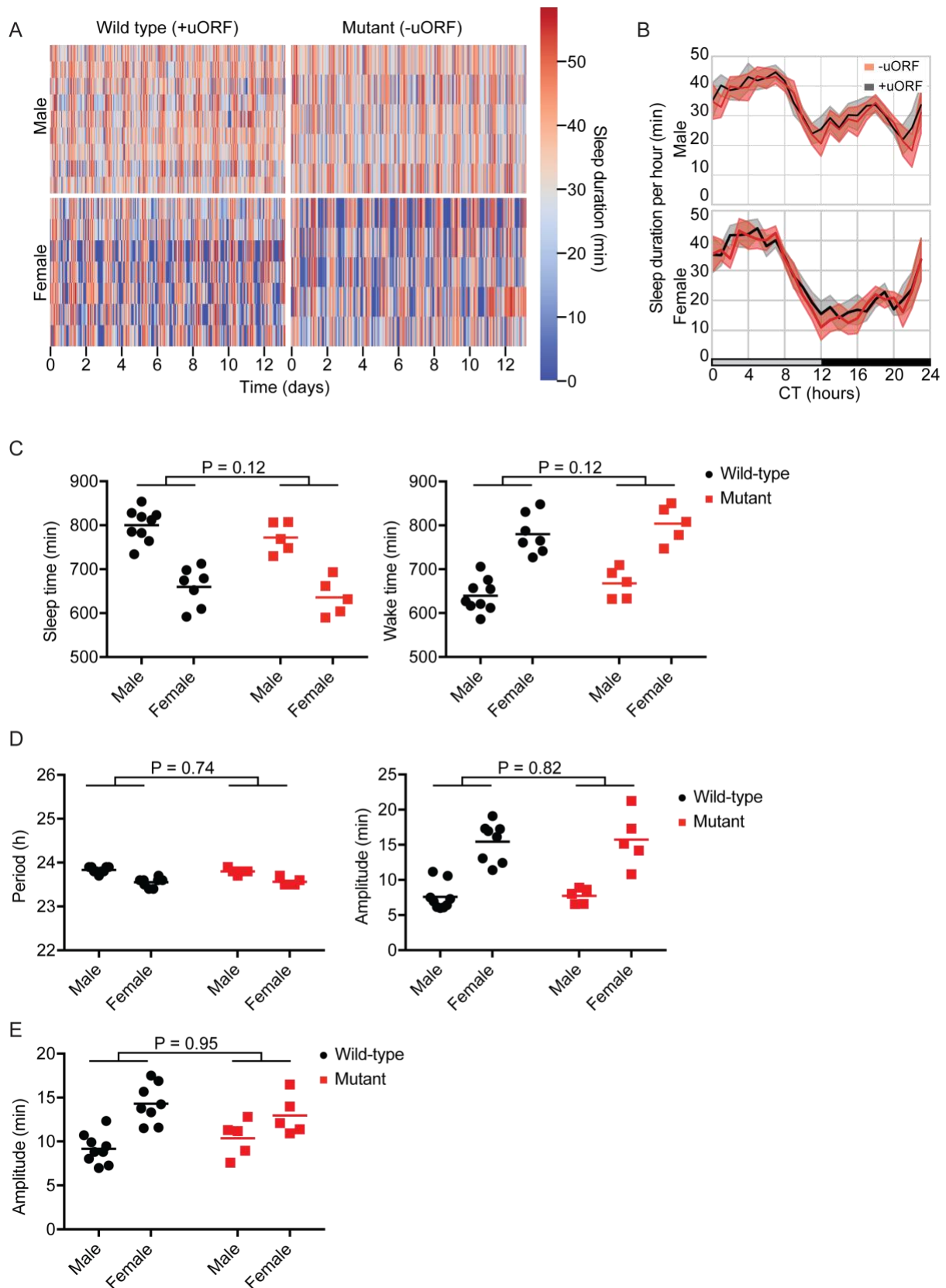
5

values, Student's unpaired t-test. (B) Sleep episode duration (*left*) was shorter and P_{sw} was

6

higher (*right*) in *Per2* uORF mutant mice than in wild-type mice, but the differences were not

1 significant. **(C)** There were no significant differences in amplitude (*left*), wake episode
2 duration (*middle*), and P_{ws} (*right*) between *Per2* uORF mutant and wild-type mice. **(D and E)**
3 Mean sleep duration per hour averaged over 13 d for 4-h windows from ZT4–8 **(D)** and ZT8–
4 12, ZT16–20, and ZT20–24 **(E)**.
5



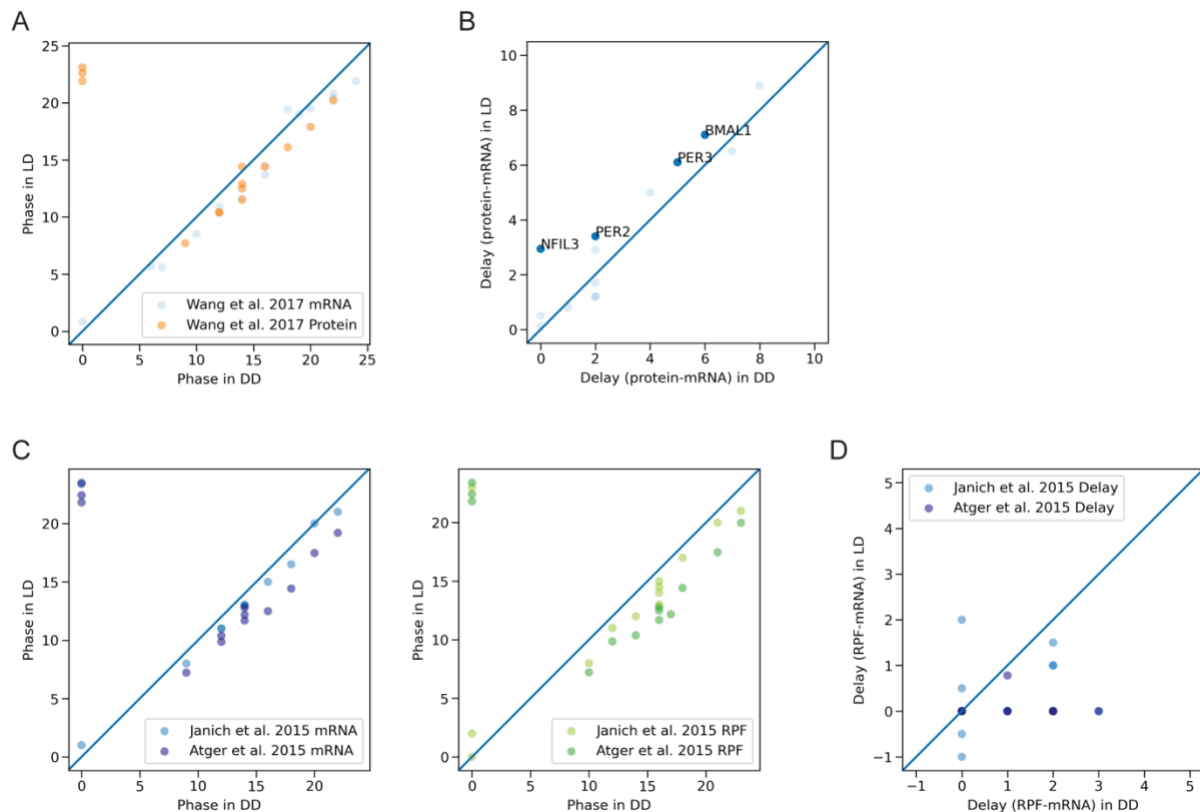
1

2 **Supplementary Figure 9 | Analysis of mice in DD conditions, and cosinor analysis of LD**

3 **and DD circadian rhythm parameters (related to Figure 4). (A) Sleep duration per hour**

4 **over 12 d in constant darkness (DD) conditions for *Per2* uORF mutant and wild-type male**

1 and female mice. Each row indicates data from one mice. **(B)** Sleep duration per hour over 24
2 h in DD, averaged over 12 d for *Per2* uORF mutant (red) and wild-type (black) male (*top*)
3 and female (*bottom*) mice. Lines indicate mean sleep duration at each time of day for each
4 strain. Shaded area, SD at each time point. **(C)** Mean sleep (*left*) and wake (*right*) duration
5 over 24 h, averaged over 12 d. Red, *Per2* uORF mutant mice. Black, wild-type. **(D)** Cosinor
6 analysis of the period (*left*) and amplitude (*right*) of wild-type and *Per2* uORF mutant mice in
7 DD conditions. **(E)** Cosinor analysis of the amplitude of wild-type and *Per2* uORF mutant
8 mice in LD conditions.
9



1
2
3
4
5
6
7
8
9
10
11

Supplementary Figure 10 | Comparison of RNA expression, translation, and protein

production phases in DD (this study) to reported phases from previously published

studies in LD conditions (6, 8, 9). (A) Protein (orange) and mRNA (blue) phases for 16

selected circadian genes observed in DD (this study) or LD (6). (B) The delay between

mRNA and protein phases observed in DD (this study) or LD (6). Several proteins (labeled)

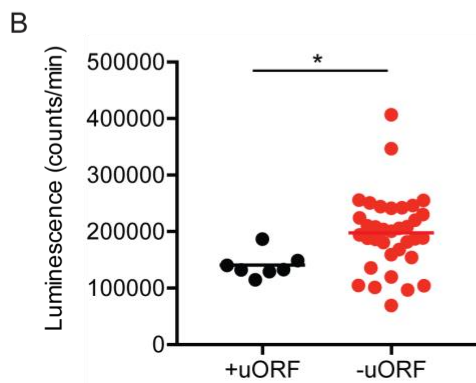
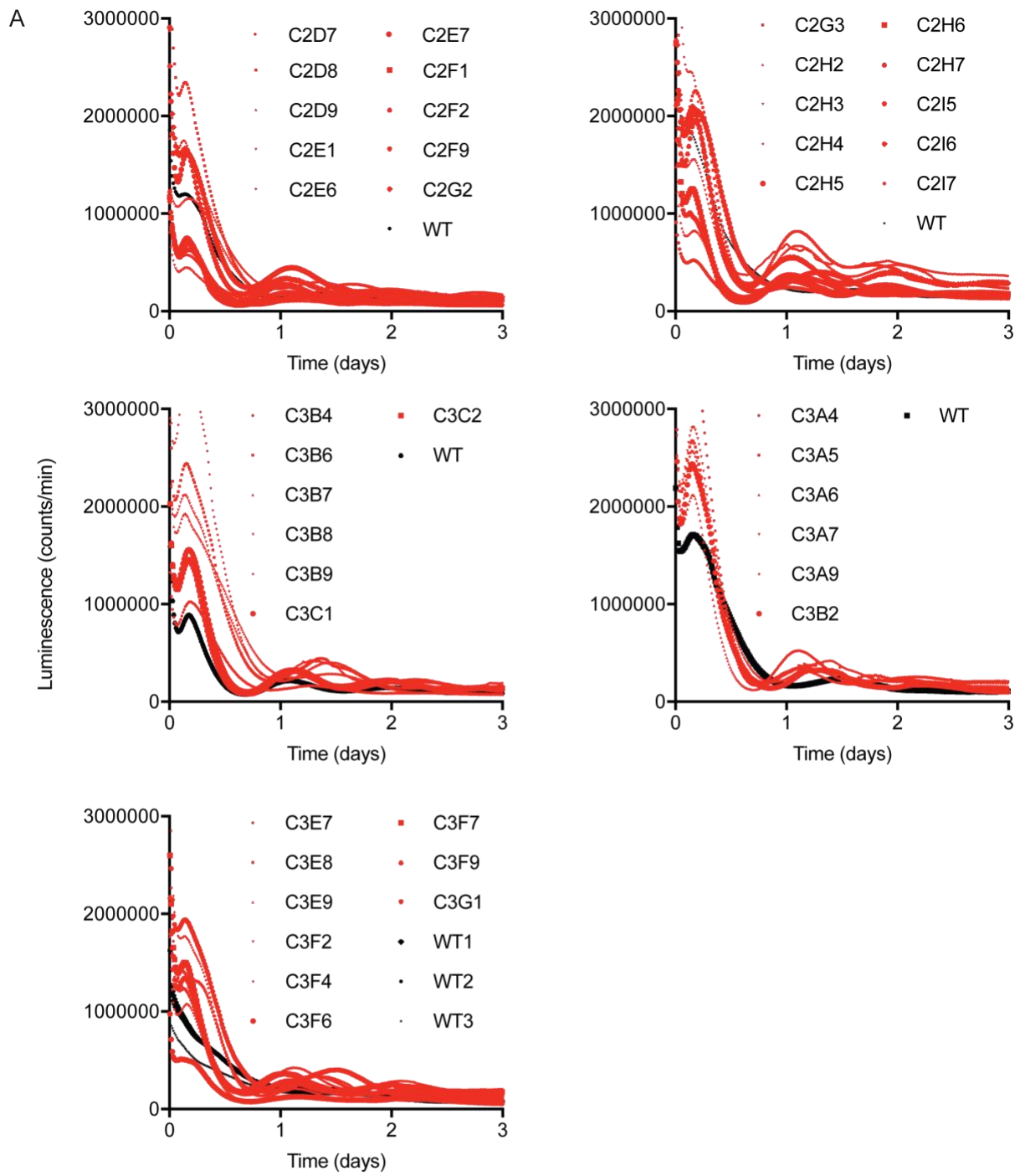
including PER2 had a greater than one hour difference in protein-mRNA delay between LD

and DD conditions. (C) The mRNA (*left*) and ribosome profiling (*right*) phases for 16

selected circadian genes observed in DD (this study) or LD (8, 9). (D) The delay between

mRNA and ribosome profiling phases observed in DD (this study) or LD (8, 9).

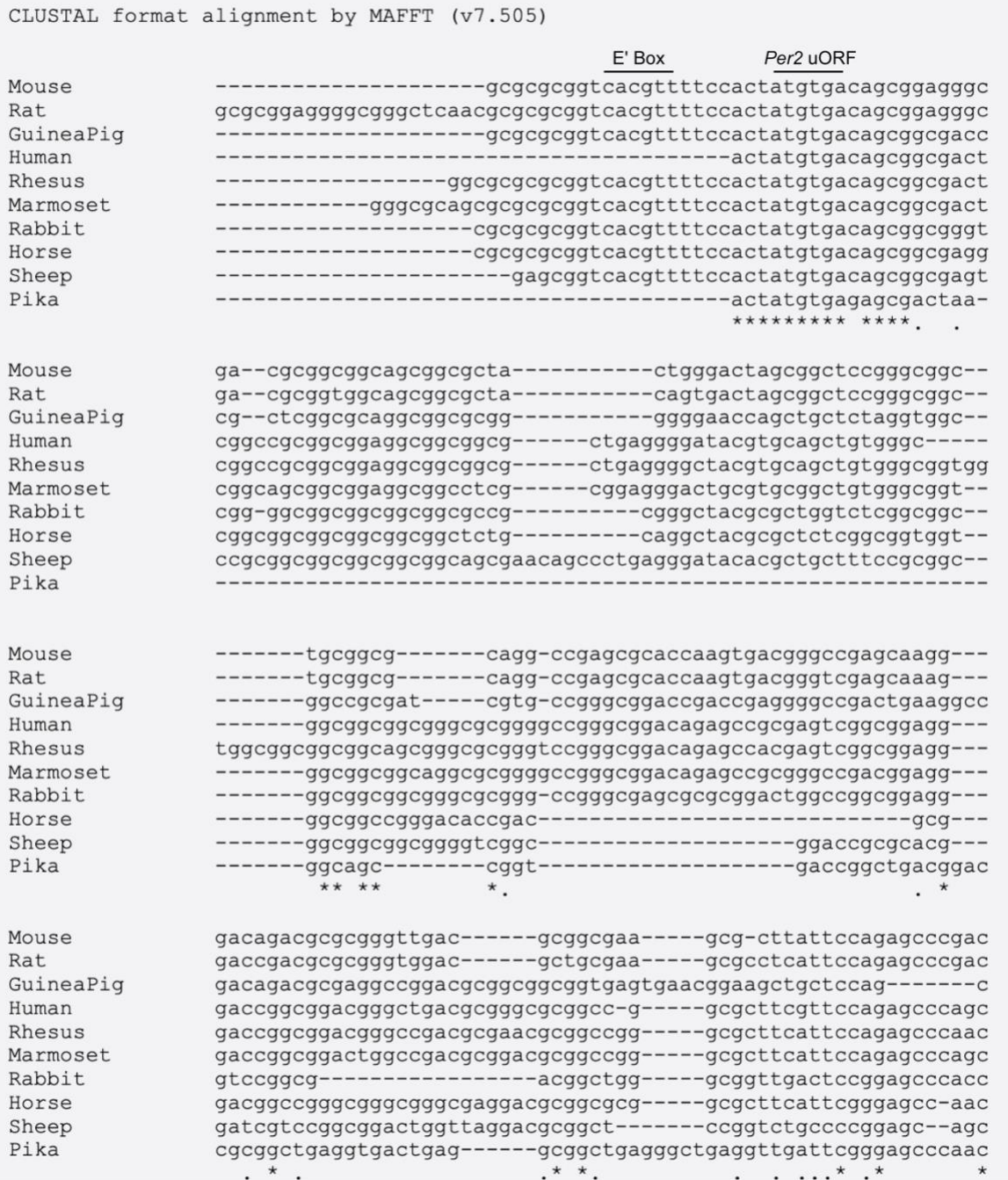
1 **Supplementary Figure 11 | Extended FACS analysis of fluorescent reporter cells with**
2 **and without the *Per2* uORF (related to Figure 3).** (A) Histogram (*left*) of GFP+ (*top*) and
3 mCherry+ (*bottom*) cells from 3T3 cells transfected with pD1-P(*Per2*)-uORF-EGFP (-uORF,
4 red) and pD1-P(*Per2*)-mCherry. (B) Histogram (*left*) of GFP+ (*top*) and mCherry+ (*bottom*)
5 cells from 3T3 cells transfected with pD1-P(*Per2*)-EGFP (+uORF, black) and pD1-P(*Per2*-
6 mCherry. The backgating strategies for each gate in (A) and (B) are shown (*right*), including
7 the percentage of GFP+ and mCherry+ cells in the population (*rightmost graph*). (C)
8 Scatterplot of GFP versus mCherry expression for -uORF (red) and +uORF (black) cells
9 gated on GFP+ expression. (D) Histogram of the GFP/mCherry ratio for cells in (C).
10



1

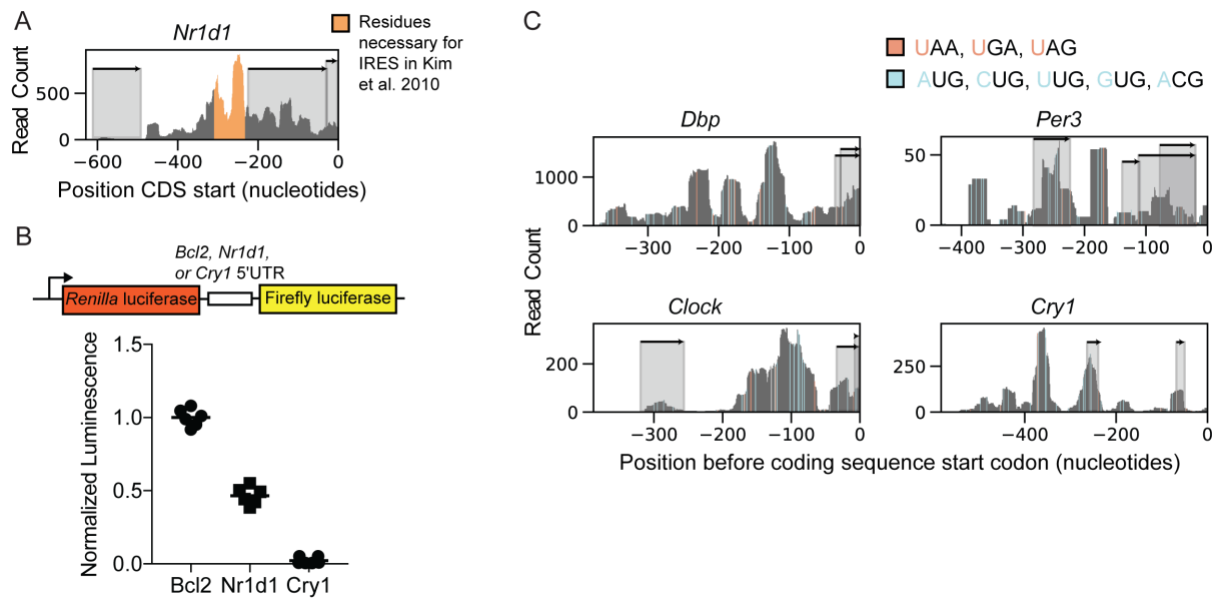
1 **Supplementary Figure 12 | Detailed analysis of the *Per2* uORF in PER2:LUC MEF**
2 **cells. (A)** Bioluminescent recordings of wild-type PER2:LUC MEF cells (black) or
3 heterozygous PER2:LUC MEF clones containing a mutated *Per2* uORF (ATGTGA to
4 GTAGGT, red). Each graph is an independent experiment performed on a different day;
5 multiple traces on the same graph indicate different clones. **(B)** Average bioluminescence
6 expression between 24 h and 72 h after dexamethasone stimulation of wild-type (black) and
7 *Per2* uORF mutant (red) MEFs.

A



1
2
3
4
5
6
7

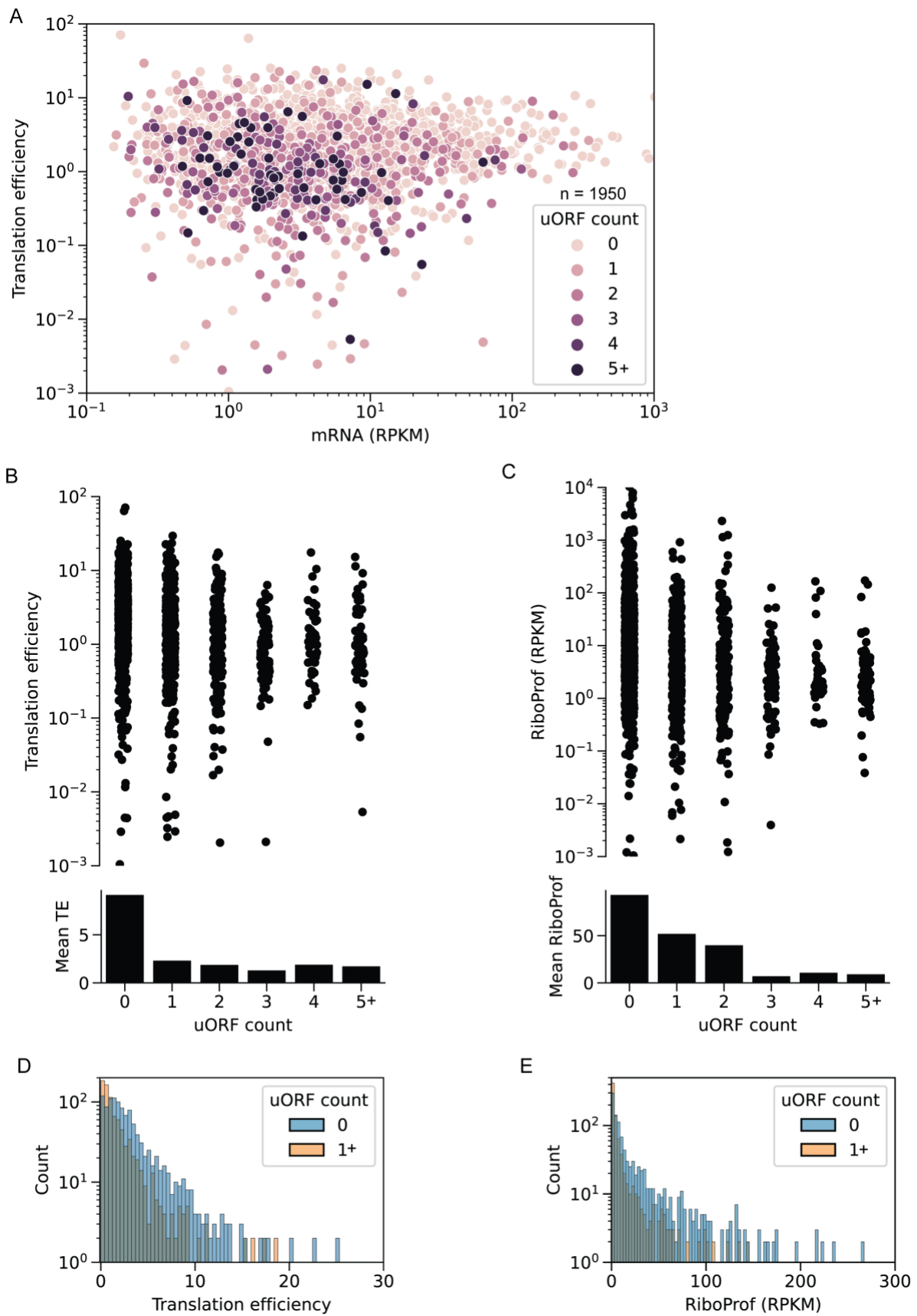
Supplementary Figure 13 | Multiple sequence alignment of the *Per2* 5'UTR. (A) Multiple sequence alignment of selected *Per2* 5'UTRs from different mammalian species using MAFFT (10). Identical nucleotides (asterisk) or pyrimidine or purine nucleotide conservation (period) among all species is shown. Note: only *Per2* transcriptional isoforms from each species containing the *Per2* uORF were used for the alignment.



1
2
3
4
5
6
7
8
9
10
11

Supplementary Figure 14 | Analysis of the IRES in the *Nr1d1* 3'UTR and distribution of near-cognate start codons and stop codons in selected 5'UTRs. (A) Extensive ribosome binding in *Nr1d1* 5' UTR overlaps with the region (orange) necessary for IRES-mediated translation of *Nr1d1* (11). (B) The efficiency of IRES-mediated translation for the *Nr1d1* 5'UTR and *Cry1* 5'UTR relative to a known IRES in *Bcl2* 5'UTR (12). (C) The 5' UTRs of *Dbp*, *Per3*, *Clock*, and *Cry1* have extensive ribosome binding in regions without a cognate uORF. Cognate and near-cognate start codons (light blue) and stop codons (orange) indicate regions of possible canonical uORFs (uORFs with an AUG start codon, shaded regions) and near-cognate uORFs (uORFs with a CUG, UUG, GUG, or ACG start codon).

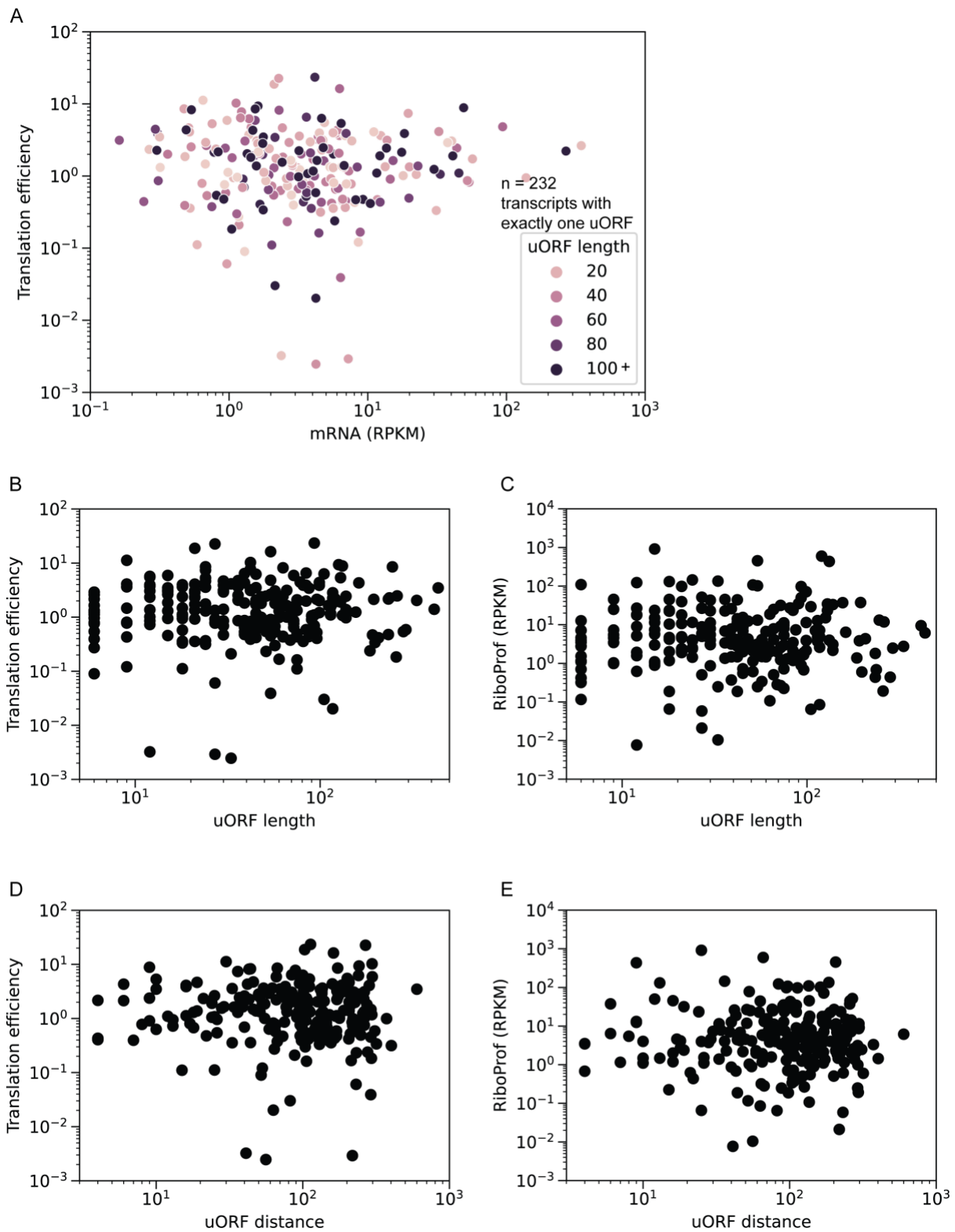
1 rev. pos. uORF, red) from the luciferase CDS. **(C)** Bioluminescent recording of 3T3 cells
2 transfected with the *Per2* short promoter without an uORF (black) or containing (red) two
3 uORFs (*left*), three uORFs (*middle*), or four uORFs (*right*). Cosinor analysis of the PMT
4 traces in **(B)** and **(C)** showing amplitude **(D)**, mesor **(E)**, and period **(F)**. **(G)** Bioluminescent
5 recording of 3T3 cells transfected with the pGL3-P(SV40)-3xE'box-dLuc containing exactly
6 one uORF, 42 nt (1x uORF, black) or 6 nt (1x rev. pos. uORF, red) from the luciferase CDS.
7 **(H)** Bioluminescent recording of 3T3 cells transfected with pGL3-P(SV40)-3xE'box-dLuc
8 without an uORF (black) or containing (red) two uORFs (*left*), three uORFs (*middle*), or four
9 uORFs (*right*). Cosinor analysis of the PMT traces in **(G)** and **(H)** showing amplitude **(I)**,
10 mesor **(J)**, and period **(K)**.
11



1

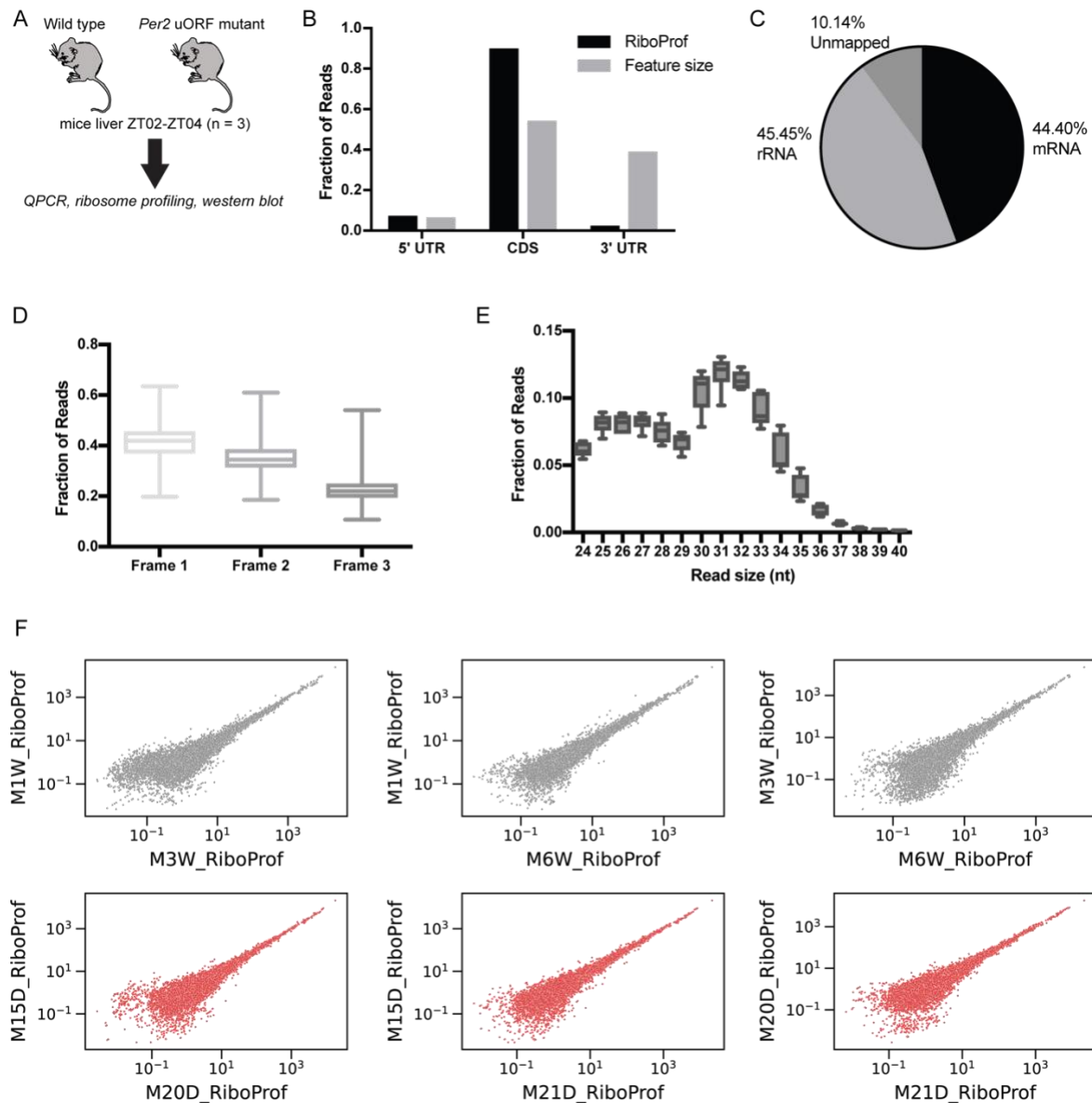
2 **Supplementary Figure 16 | Relationship between the number of uORFs and translation**
 3 **efficiency (TE) in the mouse liver using RNA-seq data from (13) and ribosome profiling**

1 **data from this study.** (A) Scatterplot of TE (mRNA RPKM from (13) divided by ribosome
2 profiling RPKM) versus transcript abundance (RPKM) colored by the number of uORFs in
3 each transcript. The distribution (*top*) and mean (*bottom*) of transcripts with the
4 corresponding number of uORFs is shown for TE (B) and ribosome binding (C). Histograms
5 of TE (D) and ribosome binding (E) for transcripts without an uORF (orange) or with one or
6 more uORFs (blue).



1
 2 **Supplementary Figure 17 | Extended analysis of translation efficiency (TE) in the mouse**
 3 **liver using RNA-seq data from (13) and ribosome profiling data from this study. (A)**
 4 Scatterplot of TE (mRNA RPKM from (13) divided by ribosome profiling RPKM) versus
 5 transcript abundance (RPKM) colored by uORF length for each transcript with exactly one

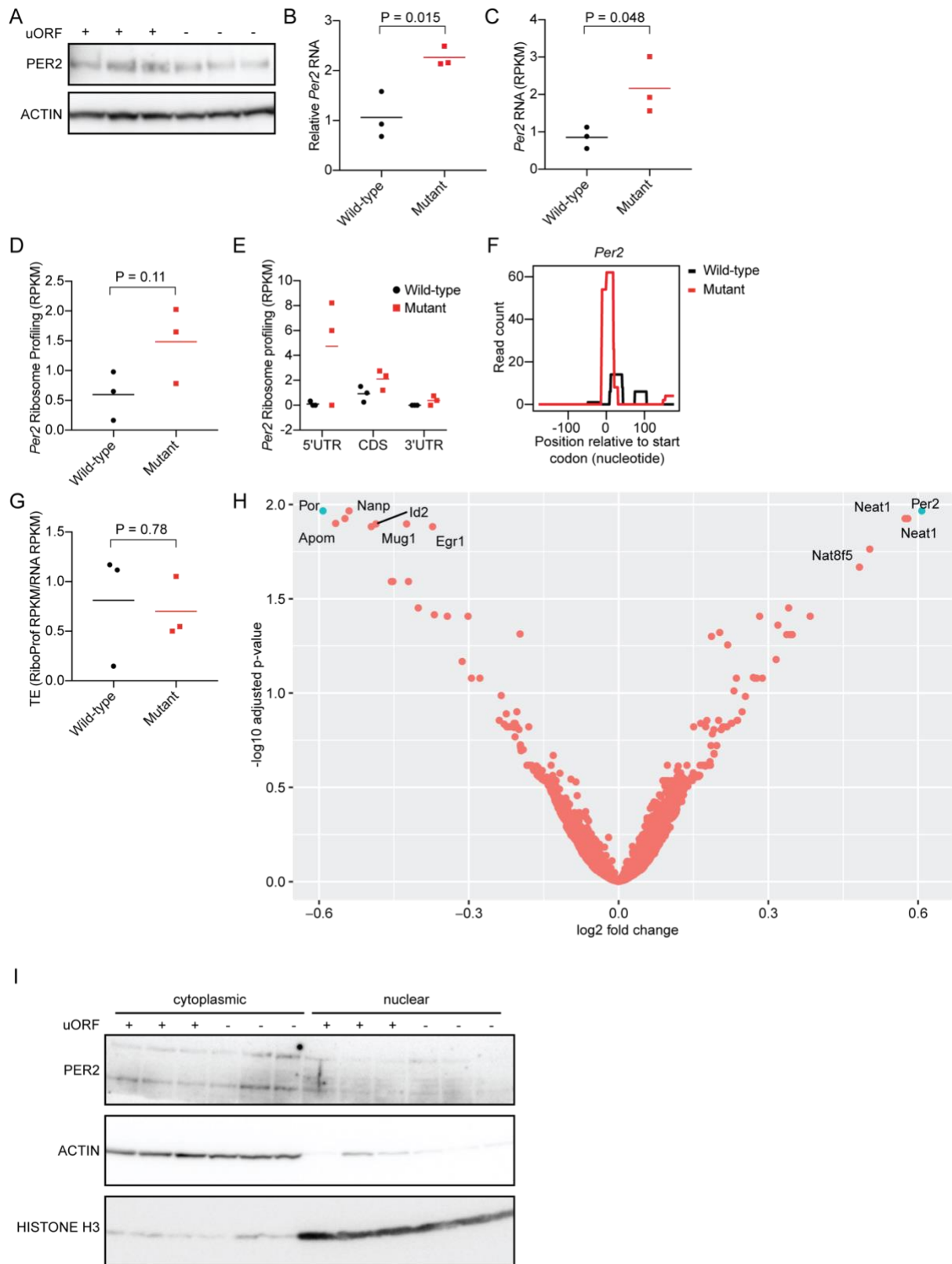
- 1 uORF. Scatterplot of TE (**B**) and ribosome binding (**C**) versus uORF length. Scatterplot of
- 2 TE (**D**) and ribosome binding (**E**) versus distance of uORF to start of the CDS.
- 3



1
2 **Supplementary Figure 18 | Validation of ribosome profiling libraries from wild-type**
3 **and *Per2* uORF mutant mice liver at ZT02-04 (related to Figure 4).** (A) Twelve to
4 fourteen-week-old male wild-type and *Per2* uORF mutant mice under LD conditions were
5 sacrificed at ZT02-ZT04 and liver sections were snap-frozen for ribosome profiling, total
6 RNA sequencing, qPCR, and western blot analyses. (B) Read distribution within 5'UTRs,
7 CDS, and 3'UTRs compared with the size of those features. Ribosome profiling reads are
8 enriched for the CDS and 5'UTR, and relatively few reads map to the 3'UTR. (C) Frame
9 analysis of ribosome profiling reads of single protein isoform mRNAs shows a preference for
10 frame 1 (the coding frame). Box-and-whisker plots: midline, median; box, 25th and 75th
11 percentiles. Whiskers are minimum and maximum values. (D) Box and whisker plots show
12 the distribution of read lengths from all sequences. The majority of reads were between 27
13 and 33 nt, which matches the footprint size of the ribosome. (E) Summary of mapped reads.

1 (F) Pairwise correlation of ribosome profiling RPKM between wild-type replicates and
2 between *Per2* uORF mutant replicates shows a high degree of correlation in ribosome
3 binding between samples.

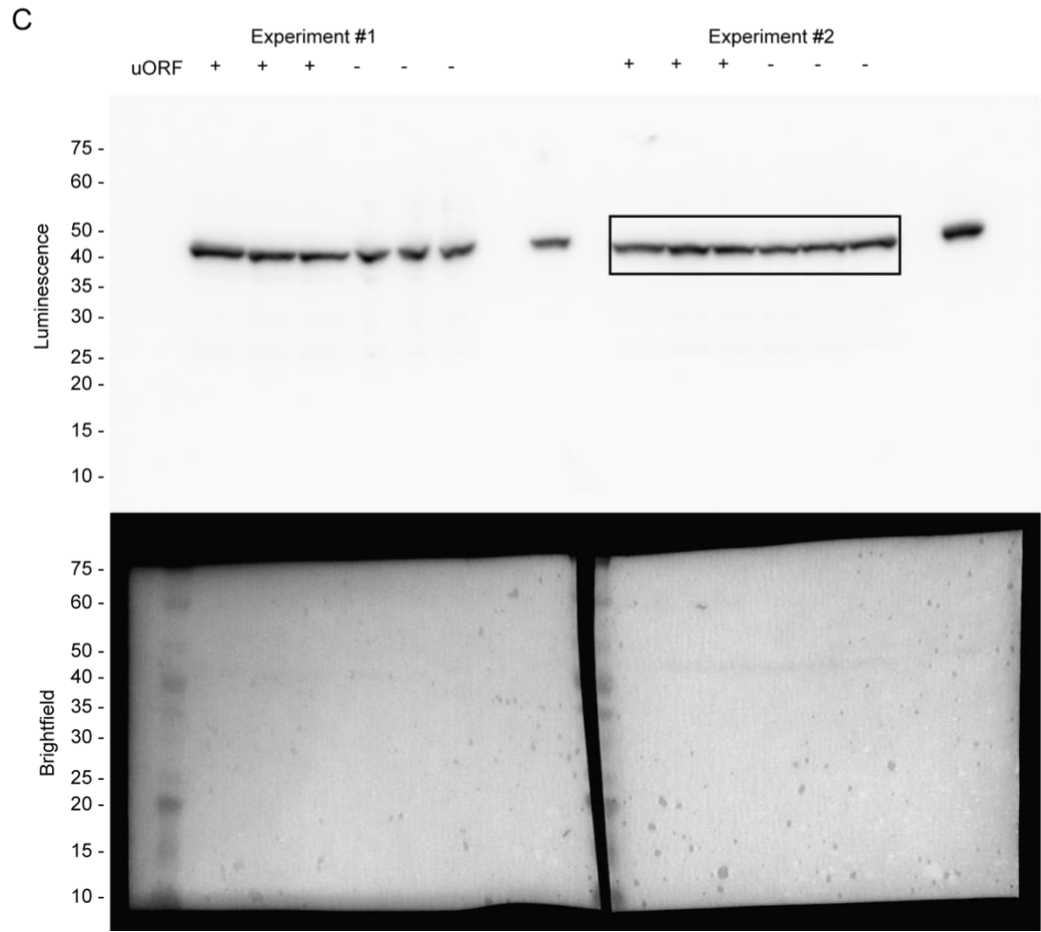
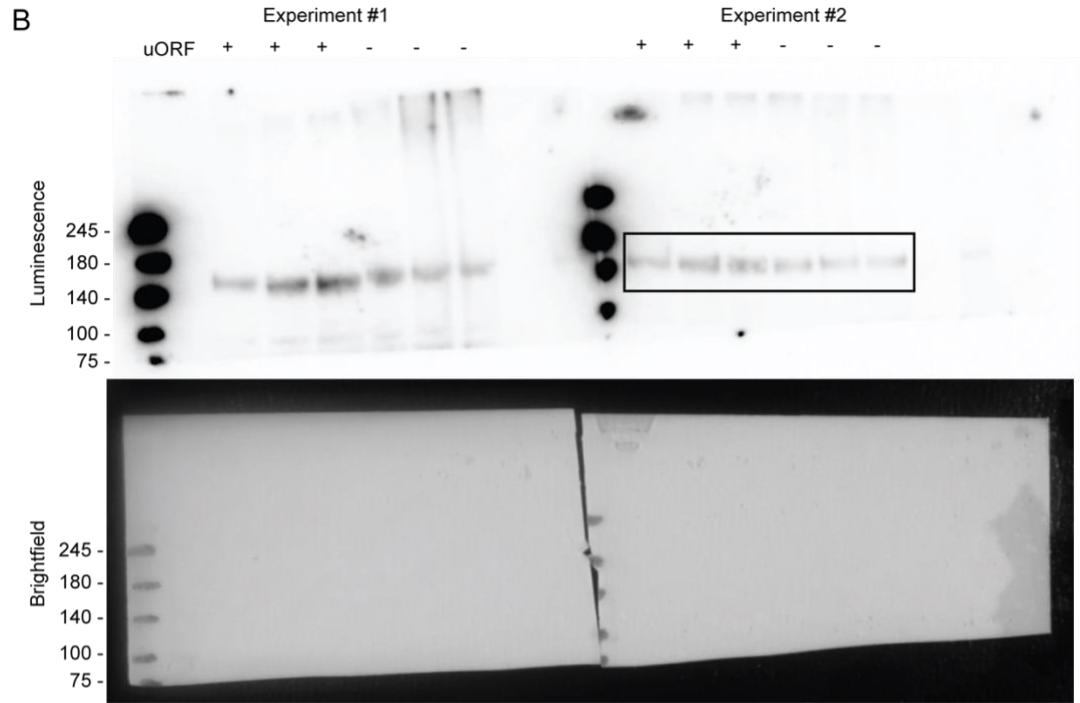
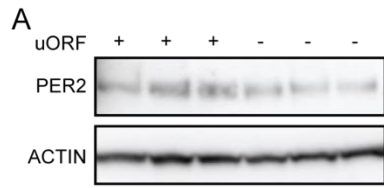
4



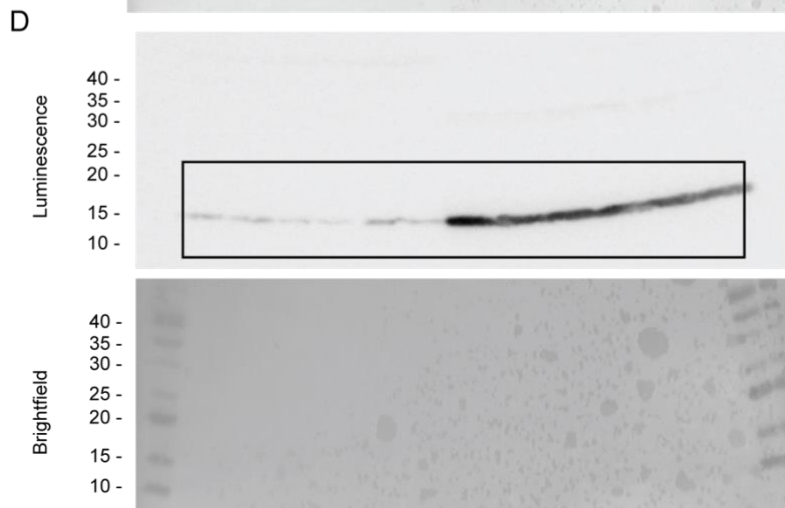
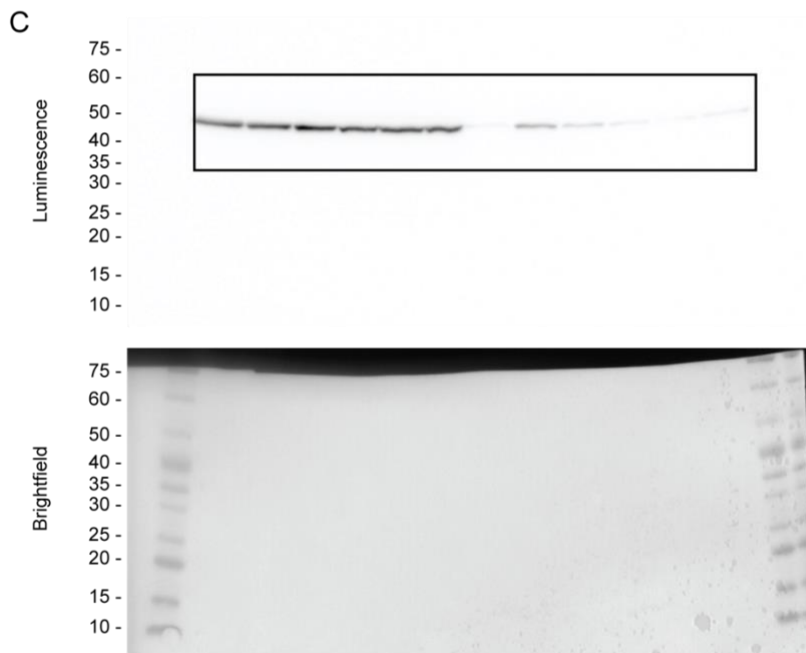
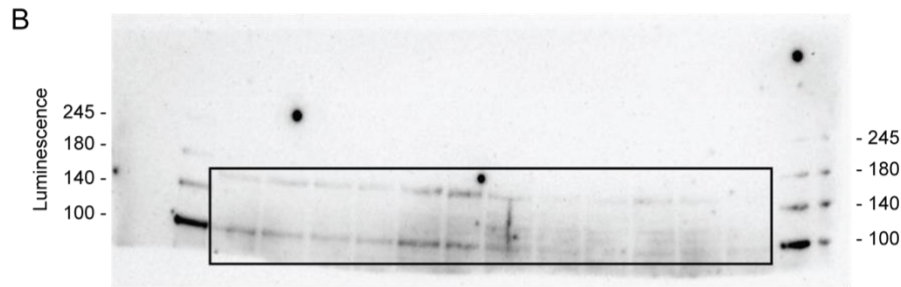
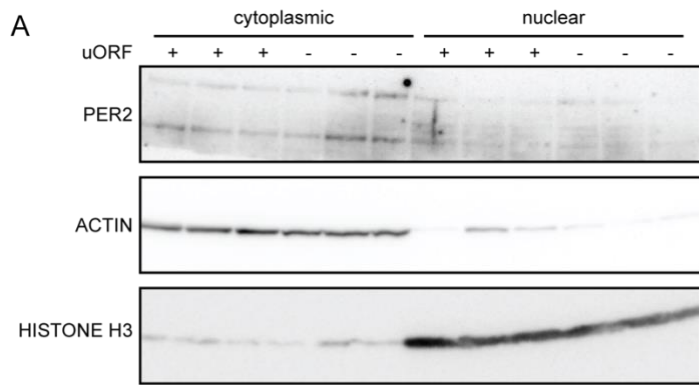
1
 2 **Supplementary Figure 19 | Ribosome profiling, RNA sequencing, qPCR, and western**
 3 **blot analysis of liver from wild-type and *Per2* uORF mutant mice at ZT02-04 (related to**
 4 **Figure 4).** (A) Western blot of PER2 and actin protein of total protein lysate from wild-type
 5 (+ uORF) and *Per2* uORF mutant (- uORF) mice liver. Expression analysis of *Per2* mRNA

1 from wild-type and *Per2* uORF mutant mice liver by qPCR (**B**) and total RNA sequencing
2 (**C**). Ribosome binding (RPKM) across the entire *Per2* transcript (**D**) or compartmentalized
3 by the 5'UTR, CDS, and 3'UTR (**E**). (**F**) Ribosome profiling reads in wild-type and *Per2*
4 uORF mutant mice in the 5'UTR. Note the absence of reads across the uORF in both samples
5 and an increased number of reads at the start codon in the *Per2* uORF mutant mice. (**G**)
6 Translation efficiency (ribosome profiling RPKM divided by total RNA RPKM) in wild-type
7 and *Per2* uORF mutant mice. (**H**) Differential expression analysis by DESeq2.0 (14)
8 indicating genes with a significant change in gene expression as defined by an adjusted p-
9 value < 0.05 and an absolute \log_2 fold change ≥ 0.58 (blue) shows that *Per2* mRNA is
10 significantly increased in *Per2* uORF mutant mice. (**I**) Immunoblot analysis of PER2, actin,
11 and histone H3 of cytoplasmic and nuclear lysates from wild-type (+ uORF) and *Per2* uORF
12 mutant (- uORF) mice liver.

13



1 **Supplementary Figure 20 | Uncropped western blot images from Fig. S19A.** (A) Cropped
2 western blot reproduced from Fig. S19A. Original uncropped images of the PER2 (B) and
3 actin (C) western blot (*top*) and brightfield image showing the molecular weight ladder
4 (*bottom*). Cropped region (black boxes).
5



1 **Supplementary Figure 21 | Uncropped western blot images from Fig. S19I.** (A) Cropped
2 western blot reproduced from Fig. S19I. Original uncropped western blot of PER2 (B) with
3 the molecular weight ladder visible in the outermost lanes. Uncropped images of actin (C)
4 and histone H3 (D) western blot (*top*) and brightfield image showing the molecular weight
5 ladder (*bottom*). Cropped region (black boxes).

1 **Table S1 | Sequence statistics for ribosome profiling data showing the circadian time**
2 **(CT), number of reads per sample, number of reads mapped to rRNA, unmapped**
3 **reads, and mapped reads.**

Sample	CT	Reads	rRNA aligned	rRNA (%)	Unmapped	Unmapped (%)	Mapped	Mapped (%)
A1	0	67420894	31637068	47	6493665	10	29290161	43
A2	4	79568956	40132748	50	6120169	8	33316039	42
A3	8	92923717	46040656	50	7305061	8	39578000	43
A4	12	89178791	37939665	43	4558237	5	46680889	52
A5	16	73866781	37993296	51	3002837	4	32870648	44
A6	20	57310601	29343482	51	3785209	7	24181910	42
A7	24	57919810	30413247	53	1903635	3	25602928	44
B1	0	82543812	46972438	57	5223484	6	30347890	37
B2	4	76767842	45784936	60	2978293	4	28004613	36
B3	8	67206206	31921429	47	2040538	3	33244239	49
B4	12	77788251	44039811	57	2632701	3	31115739	40
B5	16	73477498	42486921	58	2420565	3	28570012	39
B6	20	79546292	41792698	53	4794899	6	32958695	41
B7	24	91267817	37921444	42	20546228	23	32800145	36
Total		1066787268	544419839	51	73805521	7	448561908	42

4

1 Table S2 | JTK analysis of ribosome profiling data for circadian (BH.Q < 0.05) transcripts.

Name	RefSeq ID	BH.Q	ADJ.P	PER	LAG	AMP	CT00A	CT00B	CT04A	CT04B	CT08A	CT08B	CT12A	CT12B	CT16A	CT16B	CT20A	CT20B	CT24A	CT24B
Sigmar1	NM_001286541	0.00	1.23E-07	24	0	8.1	36.2	32.8	15.6	16.6	8.7	9.2	3.7	7.3	13.5	9.7	20.2	22.8	30.2	21.9
Tardbp	NM_145556	0.01	5.99E-07	24	0	1.2	4.9	4.2	2.3	1.7	1.1	1.0	0.3	1.0	1.9	2.0	2.4	2.7	3.9	3.1
Aqp8	NM_001109045	0.01	2.20E-06	24	0	6.5	26.2	22.8	12.4	7.4	3.4	3.1	1.0	1.4	4.3	2.3	14.2	11.4	17.9	17.4
Rdh11	NM_021557	0.01	2.20E-06	24	0	5.6	27.3	21.1	12.2	9.5	7.5	9.4	4.1	3.3	9.5	7.6	14.7	20.0	19.6	16.1
Arntl	NM_001243048	0.01	2.20E-06	24	0	2.2	4.7	4.1	2.0	2.4	0.0	0.3	0.0	0.1	1.5	1.3	2.6	3.8	3.7	3.0
Ncald	NM_001170866	0.01	2.20E-06	24	4	1.7	5.0	4.6	5.7	5.5	3.5	3.4	2.1	1.1	2.4	2.0	3.3	3.4	5.1	5.1
Ppard	NM_011145	0.01	2.20E-06	24	0	1.0	5.9	4.9	0.5	1.4	0.3	0.3	0.0	0.1	1.1	0.6	2.8	2.1	5.5	3.1
Rnf144a	NM_001081977	0.01	2.20E-06	24	0	0.6	2.9	4.1	1.3	1.3	0.6	0.5	0.0	0.2	1.0	0.7	1.9	1.0	1.7	1.9
Dennd2d	NM_001093754	0.01	2.20E-06	24	0	0.3	1.7	1.4	0.9	0.9	0.8	0.6	0.4	0.4	1.0	0.9	1.3	1.0	1.3	1.5
Pnrc1	NM_001033225	0.01	6.89E-06	24	0	25.7	59.5	68.6	43.2	40.4	16.3	11.6	11.1	8.5	34.7	16.5	34.4	44.1	44.1	49.7
Aqp8	NM_007474	0.01	6.89E-06	24	0	21.1	98.7	86.8	55.5	31.4	17.2	12.9	7.7	6.3	19.0	15.4	37.2	49.7	61.4	51.7
Pgd	NM_001081274	0.01	6.89E-06	24	0	5.6	21.4	22.5	14.4	8.9	8.5	9.1	7.1	6.7	11.9	13.7	15.2	17.2	18.2	16.0
Cks2	NM_025415	0.01	6.89E-06	24	0	3.4	28.2	22.4	13.1	11.4	6.1	8.6	2.4	6.7	10.1	9.6	12.4	10.5	16.3	13.9
Capn2	NM_009794	0.01	6.89E-06	24	0	2.0	11.3	12.4	7.7	6.4	4.6	4.8	4.3	3.0	6.1	6.6	6.5	7.4	9.4	7.9
Tjp2	NM_001198985	0.01	6.89E-06	24	0	1.2	5.2	4.0	3.3	2.4	1.6	1.9	1.6	1.0	3.1	2.2	2.6	3.5	3.7	3.3
Wee1	NM_009516	0.01	6.89E-06	24	16	1.1	0.6	0.6	0.1	0.3	2.0	1.0	2.3	2.1	3.8	2.9	1.2	1.3	0.7	0.4
Clpx	NM_001044389	0.02	1.89E-05	24	0	26.1	67.5	67.5	57.7	48.2	18.4	16.1	9.1	5.6	22.4	17.0	29.7	46.0	58.6	63.6
Nampt	NM_021524	0.02	1.89E-05	24	18	11.4	14.6	13.2	6.6	6.9	7.4	9.3	31.1	22.1	43.9	32.4	18.2	20.5	13.3	10.9
Pmvk	NM_026784	0.02	1.89E-05	24	0	6.8	40.6	32.2	9.7	7.2	4.6	5.3	4.2	4.3	8.9	9.5	18.5	24.3	23.0	16.8
Nat8	NM_023455	0.02	1.89E-05	24	22	4.2	7.1	9.3	5.8	4.3	2.7	3.3	3.3	3.1	8.4	7.6	10.2	9.8	8.8	8.5
Evi5	NM_007964	0.02	1.89E-05	24	0	2.5	11.3	13.3	9.8	8.5	5.6	5.5	5.1	2.6	7.9	6.0	6.7	8.9	9.1	9.9
Dpp9	NM_172624	0.02	1.89E-05	24	0	2.0	12.0	10.9	7.5	6.9	4.7	4.0	2.4	3.4	5.9	4.9	6.2	6.6	10.5	7.1
Tjp3	NM_001282095	0.02	1.89E-05	24	0	1.8	5.5	5.4	3.8	2.0	1.0	1.3	0.7	0.6	3.5	1.8	3.2	3.2	4.4	4.0
Bloc1s5	NM_139063	0.02	1.89E-05	24	0	1.6	13.6	11.4	8.2	7.8	6.6	5.5	4.0	5.5	7.8	6.5	7.0	8.8	10.0	8.6
Gpcpd1	NM_001042672	0.02	1.89E-05	24	12	1.5	3.0	2.4	3.8	3.2	9.1	4.8	23.0	11.7	4.5	4.3	3.0	2.9	2.1	1.9
Dock6	NM_177030	0.02	1.89E-05	24	0	0.8	3.2	2.7	1.9	1.2	0.8	0.8	0.5	0.4	1.4	1.4	1.6	2.0	2.3	1.7
Fam222a	NM_001004180	0.02	1.89E-05	24	0	0.5	2.4	3.4	0.4	1.1	0.7	0.4	0.0	0.2	0.9	0.7	1.2	1.4	2.2	1.2
Elov3	NM_007703	0.03	4.69E-05	24	1	182.4	634.0	590.9	326.6	365.0	49.3	64.1	27.1	24.1	99.2	40.9	209.9	318.8	529.0	450.4
Hacl1	NM_019975	0.03	4.69E-05	24	0	77.4	247.4	188.7	134.6	114.1	75.0	64.3	46.6	42.3	140.7	84.9	147.7	199.3	194.5	180.9
Cyp8b1	NM_010012	0.03	4.69E-05	24	2	60.6	250.8	224.1	172.1	160.4	92.1	75.7	47.1	51.5	74.6	80.9	122.2	134.5	207.2	165.3
Adck3	NM_001163290	0.03	4.69E-05	24	0	44.8	192.7	178.5	142.5	97.0	66.5	36.9	24.3	21.4	70.3	44.7	69.5	100.3	143.2	123.5
Pnp	NM_013632	0.03	4.69E-05	24	0	11.6	39.3	43.4	33.2	29.3	14.7	16.0	13.6	8.5	26.6	20.4	18.6	27.3	33.3	34.5
Dhcr7	NM_007856	0.03	4.69E-05	24	0	10.3	75.9	59.3	33.6	30.7	23.2	29.5	24.1	13.9	25.5	34.6	33.5	49.8	52.2	52.5
Efn1	NM_001162425	0.03	4.69E-05	24	0	8.6	44.0	29.9	25.3	25.9	17.4	19.4	9.0	12.3	24.4	15.1	31.6	27.2	41.9	26.6
Nr1d1	NM_145434	0.03	4.69E-05	24	10	7.0	1.3	1.3	20.9	8.1	32.1	18.8	6.8	9.2	5.6	2.0	0.7	0.8	1.5	0.8
Caprin1	NM_001111290	0.03	4.69E-05	24	0	6.3	30.6	24.1	19.0	13.9	10.1	9.5	7.6	5.9	18.6	15.5	17.9	18.0	22.7	22.9
Gale	NM_178389	0.03	4.69E-05	24	0	5.1	21.9	16.3	9.8	8.2	2.8	5.1	1.9	2.2	8.2	10.9	12.4	11.0	12.1	10.9
Avpr1a	NM_016847	0.03	4.69E-05	24	0	5.0	22.8	20.0	12.6	10.7	7.8	5.0	3.0	1.6	9.8	6.2	7.3	12.1	16.3	14.8
Asb13	NM_178283	0.03	4.69E-05	24	0	4.7	20.5	20.2	14.3	11.4	7.7	7.4	5.5	5.7	12.3	8.4	10.9	12.6	16.1	12.9
Mmab	NM_029956	0.03	4.69E-05	24	0	3.0	11.5	10.0	7.5	5.1	5.1	3.5	3.0	3.0	5.2	4.3	7.8	7.3	5.6	9.1
Rfxank	NM_001025589	0.03	4.69E-05	24	0	2.7	9.0	7.4	5.7	6.7	2.2	2.5	2.4	1.9	5.7	3.6	6.7	6.4	9.3	7.8
Lgalsl	NM_173752	0.03	4.69E-05	24	0	2.6	10.8	6.4	5.0	4.4	1.5	1.2	0.7	0.5	5.5	3.2	5.2	6.7	7.2	6.7
Chka	NM_013490	0.03	4.69E-05	24	0	2.5	7.7	6.3	4.8	5.0	1.3	1.5	0.2	0.5	3.6	2.0	2.3	4.6	6.3	5.8
Camk1d	NM_177343	0.03	4.69E-05	24	2	1.2	6.6	4.2	3.8	3.3	2.3	2.6	2.5	0.9	0.8	1.2	2.9	2.8	6.1	5.1
Per2	NM_011066	0.03	4.69E-05	24	18	1.2	2.8	1.5	0.7	0.2	1.3	1.2	2.0	2.0	6.6	4.8	3.2	2.8	2.1	1.6
St5	NM_001001326	0.03	4.69E-05	24	0	0.8	2.1	2.6	1.9	1.4	0.8	0.7	0.3	0.3	1.3	1.0	1.4	1.9	2.2	1.5
Dus2	NM_025518	0.03	4.69E-05	24	2	0.6	3.5	2.6	2.5	2.5	0.7	1.8	1.5	1.4	2.0	1.8	2.2	2.2	3.8	3.4
Slc34a2	NM_011402	0.03	4.69E-05	24	0	0.6	5.4	3.0	0.6	0.8	0.0	0.2	0.0	0.0	1.1	0.2	0.4	1.3	2.3	2.6
Ccdc151	NM_001163787	0.03	4.69E-05	24	20	0.3	0.7	0.7	0.6	0.3	0.1	0.3	0.7	0.3	1.6	0.8	0.7	1.0	0.7	0.7
Cyb5b	NM_025558	0.03	1.07E-04	24	0	50.9	283.6	239.2	169.2	130.8	106.1	82.4	75.6	67.5	149.0	97.2	126.9	148.2	194.2	173.6
Eif4ebp3	NM_201256	0.03	1.07E-04	24	18	43.8	97.9	75.0	30.9	24.6	53.1	18.2	187.2	100.8	396.5	111.1	92.3	110.7	56.6	64.6

Gys2	NM_145572	0.03	1.07E-04	24	16	22.4	45.8	41.6	31.0	21.7	58.8	36.8	85.5	70.9	103.3	86.3	40.5	53.7	39.0	36.6
Nop10	NM_025403	0.03	1.07E-04	24	0	19.1	197.0	170.9	123.8	122.5	107.9	102.6	86.0	95.2	188.9	115.7	129.7	135.0	147.9	135.6
Mrap	NM_029844	0.03	1.07E-04	24	0	13.4	54.0	47.0	33.6	24.9	16.4	14.5	12.6	12.1	35.3	19.3	35.4	28.4	33.3	41.7
Acss2	NM_019811	0.03	1.07E-04	24	0	12.6	80.3	62.4	36.2	21.1	23.1	16.3	18.3	13.5	26.8	25.7	30.0	58.4	53.5	48.8
Ppp1r3c	NM_016854	0.03	1.07E-04	24	1	10.7	77.1	39.5	25.9	24.0	12.0	11.7	11.1	4.3	18.4	9.5	19.5	38.5	62.1	56.4
Sgpl1	NM_009163	0.03	1.07E-04	24	0	7.1	30.3	22.3	21.8	15.8	13.2	11.6	9.9	6.8	19.6	17.6	15.9	21.8	24.8	25.0
Hypk	NM_026318	0.03	1.07E-04	24	0	7.0	62.3	58.0	28.7	33.7	31.7	27.0	19.0	22.6	34.5	33.4	42.5	36.9	39.9	35.7
Pter	NM_008961	0.03	1.07E-04	24	2	5.8	28.1	24.0	22.0	17.4	13.2	15.0	10.6	7.3	16.9	12.5	15.9	20.7	28.6	21.5
Tfpi2	NM_009364	0.03	1.07E-04	24	0	5.8	34.1	31.4	21.1	20.7	13.0	16.8	12.2	8.3	17.0	14.4	12.3	25.8	27.0	29.7
Slc16a1	NM_009196	0.03	1.07E-04	24	0	5.5	33.5	25.6	16.4	14.3	10.0	11.4	8.3	8.2	20.8	14.6	14.5	20.8	21.6	21.1
Tgm2	NM_009373	0.03	1.07E-04	24	0	5.4	58.5	37.5	25.8	20.6	18.1	16.3	13.1	10.9	24.7	24.1	24.2	23.2	35.4	27.5
Btg1	NM_007569	0.03	1.07E-04	24	0	5.1	16.9	16.3	11.4	7.9	6.0	5.1	3.6	2.8	9.5	3.3	6.3	12.3	12.6	13.5
Cdkn1a	NM_001111099	0.03	1.07E-04	24	0	3.9	22.0	14.0	4.5	5.7	0.4	2.3	0.5	0.6	6.6	2.6	7.8	5.7	7.6	12.4
Spryd7	NM_025697	0.03	1.07E-04	24	0	3.7	20.5	16.4	13.5	9.2	8.6	8.2	7.2	7.5	14.5	9.2	15.0	12.4	14.7	13.8
Acacb	NM_133904	0.03	1.07E-04	24	0	3.7	17.5	13.0	6.8	4.8	2.8	2.7	3.9	2.7	5.9	4.7	8.5	13.7	12.7	10.7
Pi4k2a	NM_145501	0.03	1.07E-04	24	0	3.4	17.6	16.8	14.7	10.8	8.4	8.1	5.6	7.3	13.7	9.4	10.5	12.0	15.6	14.0
Lsr	NM_001164185	0.03	1.07E-04	24	0	2.8	14.7	11.8	5.8	7.9	4.8	5.3	4.2	4.7	10.8	6.2	9.5	8.1	11.9	10.2
Ddx17	NM_001040187	0.03	1.07E-04	24	0	2.3	17.6	10.2	8.4	6.9	4.8	5.1	4.5	3.4	7.8	7.0	7.4	8.2	13.3	11.5
Ext2	NM_010163	0.03	1.07E-04	24	0	1.5	9.1	10.2	5.9	4.8	4.6	3.7	3.1	3.0	5.9	3.4	5.8	5.2	6.6	7.0
Ncoa5	NM_144892	0.03	1.07E-04	24	0	1.0	5.3	3.9	2.3	1.9	1.4	1.3	0.9	1.0	3.5	2.0	2.1	2.8	3.6	4.1
Atg7	NM_001253717	0.03	1.07E-04	24	0	0.9	6.0	5.5	4.1	3.4	2.8	2.5	2.1	2.2	4.0	3.4	3.5	3.1	4.8	4.4
Slc17a8	NM_182959	0.03	1.07E-04	24	0	0.9	3.3	3.1	2.2	1.1	0.9	0.5	0.3	0.9	1.3	1.4	2.2	1.7	2.3	1.7
Agpat5	NM_026792	0.03	1.07E-04	24	0	0.9	6.0	7.4	3.7	4.2	3.0	3.4	1.4	2.5	5.1	4.1	4.0	4.6	5.4	5.7
Rbmx	NM_001166623	0.03	1.07E-04	24	0	0.8	4.0	2.9	2.3	1.5	1.4	1.5	0.7	1.1	2.2	1.1	2.3	2.7	3.2	2.5
Dut	NM_023595	0.03	1.07E-04	24	0	0.5	5.5	4.2	2.2	2.5	2.6	2.0	0.7	1.1	2.0	2.0	5.4	2.6	3.3	3.1
Mthfr	NM_001161798	0.03	1.07E-04	24	2	0.4	1.6	1.0	1.0	0.9	0.2	0.2	0.0	0.1	0.8	0.4	0.5	0.8	1.6	1.2
Per3	NM_011067	0.03	1.07E-04	24	16	0.4	0.1	0.2	0.0	0.0	0.5	0.4	1.4	0.8	1.0	0.9	0.5	0.3	0.2	0.2
Oma1	NM_025909	0.03	1.07E-04	24	0	0.3	8.6	7.6	5.2	5.1	5.1	4.9	3.3	2.6	6.6	4.9	5.4	6.0	6.4	6.0
Mtrf1	NM_145960	0.03	1.07E-04	24	0	0.3	2.8	2.4	2.0	2.1	1.4	1.2	1.9	1.2	1.9	1.7	2.1	2.0	2.3	2.5
St5	NM_029811	0.03	1.07E-04	24	2	0.2	0.3	0.4	0.1	0.2	0.1	0.1	0.0	0.0	0.1	0.0	0.4	0.2	0.4	0.4
Plekhg1	NM_001033253	0.03	1.07E-04	24	0	0.1	0.8	0.8	0.5	0.6	0.4	0.3	0.5	0.3	0.5	0.5	0.6	0.6	0.7	0.7
Eif2ak4	NM_013719	0.03	1.07E-04	24	0	0.1	0.5	0.6	0.2	0.2	0.1	0.1	0.1	0.1	0.3	0.2	0.5	0.3	0.4	0.3
Creb3l1	NM_011957	0.03	1.07E-04	24	0	0.1	0.4	0.6	0.2	0.2	0.1	0.1	0.1	0.1	0.3	0.2	0.2	0.3	0.3	0.3
Prdm10	NM_001080817	0.03	1.07E-04	24	0	0.1	0.5	0.6	0.3	0.4	0.4	0.3	0.2	0.2	0.3	0.3	0.4	0.4	0.5	0.4
Bhmt	NM_016668	0.05	2.29E-04	24	0	57.1	362.2	255.4	289.4	185.9	124.4	119.1	114.4	86.9	175.5	136.1	138.8	248.3	245.3	318.2
Plin2	NM_007408	0.05	2.29E-04	24	2	46.8	236.4	188.9	145.4	159.6	137.3	93.5	56.2	66.7	118.5	90.0	106.9	141.7	195.0	145.1
S100a10	NM_009112	0.05	2.29E-04	24	0	42.9	251.9	240.6	210.9	169.6	110.4	111.9	94.9	66.3	153.0	110.9	128.9	160.6	191.6	193.6
Cyb5r3	NM_029787	0.05	2.29E-04	24	0	35.4	317.2	278.3	210.4	187.7	184.2	160.3	157.6	146.6	258.5	188.5	190.8	233.0	253.0	235.9
Sdc1	NM_011519	0.05	2.29E-04	24	0	33.1	203.0	165.9	96.1	85.7	60.3	47.8	63.9	46.1	144.9	71.1	107.8	105.6	129.4	117.2
Tubb2a	NM_009450	0.05	2.29E-04	24	0	29.5	79.5	60.2	51.5	36.8	5.7	9.8	4.8	2.4	37.9	17.9	27.2	39.2	83.6	51.2
Ddc	NM_001190448	0.05	2.29E-04	24	0	19.3	81.0	59.3	45.5	47.0	18.4	22.2	13.2	12.9	54.8	37.3	43.1	56.8	52.4	55.4
Gclc	NM_010295	0.05	2.29E-04	24	2	16.2	66.9	71.1	60.3	51.2	44.5	29.1	26.7	23.5	35.5	28.3	31.7	44.7	63.3	54.3
Tars	NM_033074	0.05	2.29E-04	24	0	15.6	62.1	52.9	43.9	33.1	20.1	18.8	14.3	12.7	35.3	27.6	26.4	40.9	49.9	40.4
Pnkd	NM_001039509	0.05	2.29E-04	24	0	12.5	46.8	41.1	32.1	22.8	14.5	9.8	9.1	6.7	30.0	14.6	21.8	25.1	35.1	26.7
Hmgcs1	NM_145942	0.05	2.29E-04	24	0	11.2	62.0	58.9	37.6	26.4	23.5	41.8	16.9	10.5	25.0	21.7	31.3	56.0	57.4	54.0
Cldn2	NM_016675	0.05	2.29E-04	24	0	11.0	49.0	42.0	35.3	31.6	20.9	19.7	14.2	16.8	32.8	20.6	19.7	37.2	38.8	35.5
Acsl4	NM_001033600	0.05	2.29E-04	24	20	10.4	31.2	26.2	18.7	17.0	14.2	16.6	23.7	16.2	31.7	35.1	30.2	38.0	29.8	27.1
Adh4	NM_011996	0.05	2.29E-04	24	2	9.8	57.5	58.3	51.4	43.1	43.5	42.5	32.3	22.4	42.4	37.5	30.9	51.7	58.5	64.0
Ran	NM_009391	0.05	2.29E-04	24	0	8.6	63.1	52.5	34.4	25.9	21.7	23.6	20.5	21.5	36.9	28.7	26.9	33.8	50.7	38.4
Fdft1	NM_010191	0.05	2.29E-04	24	0	6.2	22.9	21.4	7.1	7.5	6.6	13.6	6.4	4.2	10.7	11.3	15.4	17.9	19.6	18.6
Mal2	NM_178920	0.05	2.29E-04	24	0	5.7	24.9	24.0	11.4	9.4	5.8	4.8	4.2	6.9	22.2	9.2	14.9	13.8	17.8	18.0
Atg101	NM_026566	0.05	2.29E-04	24	0	5.4	28.0	24.8	20.2	16.7	12.8	11.9	7.2	8.3	18.9	11.0	13.9	17.0	22.8	21.1
2610528J11Rik	NM_025572	0.05	2.29E-04	24	0	4.9	16.4	16.6	13.3	9.9	10.3	5.5	5.4	3.6	9.4	6.4	7.9	11.6	13.5	14.1
Lpin1	NM_001130412	0.05	2.29E-04	24	15	4.3	3.8	3.6	2.7	1.9	7.2	7.3	66.9	50.2	17.8	15.8	5.1	4.0	3.4	2.8
Ubqln1	NM_152234	0.05	2.29E-04	24	0	3.9	29.4	29.1	21.9	19.8	16.6	14.5	14.1	12.6	28.3	18.5	21.0	21.0	25.9	23.5
Nmrk1	NM_145497	0.05	2.29E-04	24	18	3.9	6.0	5.5	3.5	4.3	3.9	3.4	14.9	9.5	16.2	11.6	7.0	7.2	4.5	5.5

Anp32a	NM_009672	0.05	2.29E-04	24	0	3.4	39.8	39.6	29.9	21.8	20.0	17.0	19.8	15.4	21.0	20.0	17.3	31.3	37.0	32.9
Ppm1b	NM_001159496	0.05	2.29E-04	24	0	2.9	16.6	16.0	13.9	9.3	10.3	7.2	8.3	5.6	12.5	8.9	11.1	11.7	15.7	14.5
Tnfrap2	NM_009396	0.05	2.29E-04	24	1	2.8	10.6	8.3	7.3	6.6	4.0	2.8	2.5	1.4	4.3	2.6	4.7	5.7	8.0	6.4
Tlcd1	NM_026708	0.05	2.29E-04	24	18	2.7	7.5	4.4	4.9	3.9	6.0	5.0	8.1	6.4	10.6	8.7	9.0	8.4	7.1	6.2
Pabpn1	NM_019402	0.05	2.29E-04	24	0	2.6	15.8	14.0	10.4	8.2	7.5	6.8	5.5	5.6	12.6	7.6	9.5	13.2	13.2	8.6
Tspan33	NM_146173	0.05	2.29E-04	24	0	2.3	9.3	8.4	7.2	5.7	4.6	3.7	3.6	3.1	5.6	3.5	6.7	5.0	7.0	8.0
Acnat1	NM_001164565	0.05	2.29E-04	24	0	2.1	11.9	10.6	7.1	6.3	4.9	3.7	3.3	2.3	7.8	6.8	4.9	7.9	10.9	8.0
40057	NM_001113487	0.05	2.29E-04	24	0	2.1	11.8	10.4	7.7	6.8	5.2	4.3	3.3	2.3	7.9	6.4	8.1	7.7	9.1	7.3
Lpin2	NM_022882	0.05	2.29E-04	24	14	2.1	4.4	4.9	3.6	3.8	6.8	5.6	10.9	8.6	8.9	7.8	4.9	5.4	4.0	2.9
Mtap	NM_024433	0.05	2.29E-04	24	0	2.0	16.0	14.0	7.4	7.6	6.5	6.1	5.6	4.8	11.2	6.1	7.8	10.2	10.1	13.9
Taf15	NM_027427	0.05	2.29E-04	24	0	1.7	17.6	14.4	8.6	6.8	6.1	7.2	8.0	5.6	9.2	8.6	9.6	10.4	13.6	9.6
Rpa1	NM_001164223	0.05	2.29E-04	24	0	1.5	11.6	10.2	8.1	6.3	5.0	6.2	5.4	4.6	6.0	6.9	6.0	7.7	9.5	8.3
Lnx2	NM_080795	0.05	2.29E-04	24	0	1.4	7.3	6.8	3.8	3.7	2.1	2.1	1.3	1.5	6.5	3.2	4.1	3.4	5.9	4.3
Gca	NM_145523	0.05	2.29E-04	24	0	1.2	3.6	5.4	2.9	2.5	1.3	1.5	0.1	1.2	2.3	2.3	3.1	2.5	2.0	4.0
Bco2	NM_133217	0.05	2.29E-04	24	0	1.1	6.2	6.3	4.2	3.3	4.1	2.7	1.9	1.7	3.0	2.8	2.9	4.6	5.8	4.5
Itgb5	NM_001145884	0.05	2.29E-04	24	0	0.9	8.4	6.8	4.1	4.5	3.4	2.8	3.2	2.2	4.8	3.4	3.5	4.8	6.4	5.2
Sorbs2	NM_001205219	0.05	2.29E-04	24	0	0.9	5.1	4.3	3.9	3.9	3.0	3.2	2.0	1.7	4.6	3.3	4.1	4.8	5.0	4.2
Arntl	NM_007489	0.05	2.29E-04	24	0	0.9	2.3	2.9	2.1	1.2	0.2	0.2	0.3	0.0	0.7	0.8	1.0	1.5	2.1	1.0
40787	NM_001009818	0.05	2.29E-04	24	0	0.7	5.0	4.3	3.2	2.3	1.9	2.2	1.6	1.1	2.4	4.4	3.2	3.3	3.4	4.0
Shkbp1	NM_138676	0.05	2.29E-04	24	0	0.7	2.7	2.3	1.7	1.5	1.1	0.9	1.0	0.9	1.7	1.1	2.1	1.6	2.0	1.7
Syne1	NM_001079686	0.05	2.29E-04	24	4	0.5	1.4	1.8	2.1	1.5	1.1	0.8	0.6	0.3	0.6	0.5	0.6	1.0	1.8	1.7
Rad9a	NM_011237	0.05	2.29E-04	24	22	0.5	1.4	1.1	0.6	0.6	0.1	0.2	0.3	0.3	0.8	0.7	1.0	1.0	1.3	0.7
Smarcal1	NM_018817	0.05	2.29E-04	24	0	0.4	3.5	3.3	2.3	2.1	1.7	1.5	0.9	1.0	2.0	2.1	1.9	2.1	2.8	2.3
Gtf3c5	NM_148928	0.05	2.29E-04	24	0	0.4	3.9	2.5	1.8	1.8	1.4	1.4	0.7	1.1	1.6	1.4	1.4	2.2	2.4	1.7
Ptpn9	NM_019651	0.05	2.29E-04	24	0	0.3	3.3	2.3	1.3	1.6	0.8	1.1	1.0	1.1	1.9	1.1	1.3	2.3	2.1	2.9
Ddhd1	NM_001039106	0.05	2.29E-04	24	0	0.3	2.1	1.9	0.9	1.0	0.6	0.6	0.8	0.5	1.4	0.8	0.9	1.1	1.5	1.4
E4f1	NM_007893	0.05	2.29E-04	24	0	0.3	1.3	0.9	0.6	0.6	0.4	0.5	0.4	0.3	0.8	0.5	1.0	0.8	1.1	0.7
Sorbs2	NM_172752	0.05	2.29E-04	24	0	0.2	2.2	2.6	1.8	1.4	1.4	1.6	0.9	0.9	1.7	1.5	1.5	2.0	2.0	2.1
Opn3	NM_010098	0.05	2.29E-04	24	0	0.1	0.8	0.6	0.1	0.2	0.1	0.2	0.0	0.0	0.3	0.1	0.2	0.3	0.4	0.5

Table S3 | Sequence statistics for ribosome profiling data for wild-type (M1W, M3W, M6W) and *Per2* uORF mutant (M15, M20D, M21D) showing the number of reads per sample, number of reads mapped to rRNA, unmapped reads, and mapped reads.

Sample	Reads	rRNA aligned	rRNA (%)	Unmapped	Unmapped (%)	Mapped	Mapped (%)
M1W	31067707	13722226	44	3495502	11	13849979	45
M3W	30481515	12873480	42	3235911	11	14372124	47
M6W	37574250	18179097	48	3539752	9	15855401	42
M15D	38245244	18128177	47	3624572	9	16492495	43
M20D	42932671	19864776	46	4212170	10	18855725	44
M21D	33744849	14525219	43	3601489	11	15618141	46

Dataset S1 (separate file). JTK analysis of ribosome profiling data for all transcripts.

Dataset S2 (separate file). JTK analysis of ribosome profiling data for all uORFs.

Dataset S3 (separate file). Translation efficiency using RNA-seq data from (13) and ribosome profiling data from this study.

Dataset S4 (separate file). Ribosome profiling, total RNA sequencing, and translation efficiency from the livers of three wild-type (M1W, M3W, and M6W) and three *Per2* uORF mutant (M15D, M20D, and M21D) mice sacrificed at ZT02-04.

Dataset S5 (separate file). Differential expression analysis of total RNA from the livers of three wild-type (M1W, M3W, and M6W) and three *Per2* uORF mutant (M15D, M20D, and M21D) mice sacrificed at ZT02-04.

SI References

1. T. K. Sato, *et al.*, Feedback repression is required for mammalian circadian clock function. *Nat. Genet.* **38**, 312–319 (2006).
2. M. Ukai-Tadenuma, *et al.*, Delay in feedback repression by cryptochrome 1 is required for circadian clock function. *Cell* **144**, 268–281 (2011).
3. Y. Isojima, *et al.*, CK1 ϵ / δ -dependent phosphorylation is a temperature-insensitive, period-determining process in the mammalian circadian clock. *Proc. Natl. Acad. Sci.* (2009) <https://doi.org/10.1073/pnas.0908733106> (August 31, 2011).
4. B. Langmead, S. L. Salzberg, Fast gapped-read alignment with Bowtie 2. *Nat. Methods* **9**, 357–359 (2012).
5. F. A. Ran, *et al.*, Genome engineering using the CRISPR-Cas9 system. *Nat. Protoc.* **8**, 2281–2308 (2013).
6. J. Wang, *et al.*, Nuclear Proteomics Uncovers Diurnal Regulatory Landscapes in Mouse Liver. *Cell Metab.* **25**, 102–117 (2017).
7. R. Narumi, *et al.*, Mass spectrometry-based absolute quantification reveals rhythmic variation of mouse circadian clock proteins. *Proc. Natl. Acad. Sci. U. S. A.* **113**, E3461-3467 (2016).
8. F. Atger, *et al.*, Circadian and feeding rhythms differentially affect rhythmic mRNA transcription and translation in mouse liver. *Proc. Natl. Acad. Sci. U. S. A.* **112**, E6579-6588 (2015).
9. P. Janich, A. B. Arpat, V. Castelo-Szekely, M. Lopes, D. Gatfield, Ribosome profiling reveals the rhythmic liver translome and circadian clock regulation by upstream open reading frames. *Genome Res.* **25**, 1848–1859 (2015).
10. K. Katoh, J. Rozewicki, K. D. Yamada, MAFFT online service: multiple sequence alignment, interactive sequence choice and visualization. *Brief. Bioinform.* **20**, 1160–1166 (2019).

11. D.-Y. Kim, K.-C. Woo, K.-H. Lee, T.-D. Kim, K.-T. Kim, hnRNP Q and PTB modulate the circadian oscillation of mouse Rev-erb alpha via IRES-mediated translation. *Nucleic Acids Res.* **38**, 7068–7078 (2010).
12. K. W. Sherrill, M. P. Byrd, M. E. Van Eden, R. E. Lloyd, BCL-2 translation is mediated via internal ribosome entry during cell stress. *J. Biol. Chem.* **279**, 29066–29074 (2004).
13. N. Koike, *et al.*, Transcriptional architecture and chromatin landscape of the core circadian clock in mammals. *Science* **338**, 349–354 (2012).
14. M. I. Love, W. Huber, S. Anders, Moderated estimation of fold change and dispersion for RNA-seq data with DESeq2. *Genome Biol.* **15**, 550 (2014).